ON VACUUM FIELD PROPERTIES OF THE URAGAN-2M TORSATRON STANDARD CONFIGURATION

V. E. Bykov and A. A. Shishkin [1)]

and

J. Kißlinger and F. Rau [2)]

IPP 2/301 August 1989

MAX-PLANCK-INSTITUT FÜR PLASMAPHYSIK

8046 GARCHING BEI MÜNCHEN

MAX-PLANCK-INSTITUT FÜR PLASMAPHYSIK
Garching bei München

ON VACUUM FIELD PROPERTIES OF THE URAGAN-2M TORSATRON STANDARD CONFIGURATION

V. E. Bykov and A. A. Shishkin [1)]
and
J. Kißlinger and F. Rau [2)]

IPP 2/301 August 1989

[1)] Kharkov Institute of Physics and Technology
Ukrainian Academy of Sciences, USSR
[2)] Max-Planck-Institut für Plasmaphysik
D-8046 Garching, FRG, EURATOM Association

Die nachstehende Arbeit wurde im Rahmen des Vertrages zwischen dem Max-Planck-Institut für Plasmaphysik und der Europäischen Atomgemeinschaft über die Zusammenarbeit auf dem Gebiet der Plasmaphysik durchgeführt.

Table of contents

ABSTRACT

Vacuum field properties of the URAGAN-2M Torsatron are investigated. In the 'Standard Case', within a certain range of field parameters, the size of the observed magnetic islands at $\iota = 2/3$ can be reduced considerably. Some characteristic quantities for stellarator vacuum fields are reported.

1.) INTRODUCTION

The present IPP-Report describes vacuum field properties for the 'Standard Case' of the URAGAN-2M Torsatron. This experiment, sometimes abbreviated with cyrillic letters $\mathcal{Y}2M$, is under construction /1/ at the Kharkov Institute of Physics and Technology of the Ukrainian Academy of Sciences, USSR. The design value of the magnetic field is $B_o = 2$ T, the major radius of the system is 1.7 m, the plasma aspect ratio is about 10. Some details of the coil systems of the device are given in section 2 : the helical windings are of $\ell = 2,4$ type with $M = 4$ field periods, utilizing a particular winding law. In addition to axisymmetric compensation and correction windings, a set of 16 toroidal field coils is foreseen. They produce the major part of the toroidal field and thus reduce effects of the helical ripple. These four coil systems provide a certain range of vacuum field parameters. In section 3, results of recent calculations are presented for the URAGAN-2M Standard Case. They were obtained at IPP Garching by numerical field line integration using the Gourdon code. The vacuum field shows a number of 'natural' magnetic islands at rational ι-values. The largest islands are situated near the edge at $\iota = 2/3$. As described in section 4, the size of these islands can be reduced considerably by a change of a small parameter in the winding law. Simultaneously the size of the last useful flux surface is increased. These results are also valid at other ι-values, when the 2/3-islands have been shifted by a small amount, while keeping the axis position approximately constant. In section 5, some useful characteristic quantities evaluated from the vacuum fields are given for the Standard Case of URAGAN-2M and for the configuration with compensated islands at $\iota = 2/3$. Section 6 is a short summary with conclusions.

2.) URAGAN-2M COIL SYSTEMS

The experimental device URAGAN-2M is a torsatron with $M = 4$ field periods and utilizes four different coil systems :

- two $\ell = 2$ helical windings, HF-1 and HF-2, where each 'pole' is split into two 'half-poles' in order to provide some $\ell = 4$ harmonics;
- eight axisymmetric compensation windings VF-1 to VF-8, which balance the vertical field of the helical windings;
- four correction windings C-1 to C-4, which allow an additional shift of the magnetic axis;
- a set of 16 toroidal field coils TF-1 to TF-16, situated in the radial space between the helical windings and the vertical field coils; see Figure 1 .

These coil systems are described separately in the following, along with some information pertaining to the present numerical field calculations.

Toroidal Field Coils

The major part of the toroidal field in the 'Standard Case' of URAGAN-2M is produced by a set of 16 circular coils. The outer radius of each coil is $a_{t2} = 77.9$ cm, the inner radius is $a_{t1} = 59.3$ cm, the cylindrical length is $h_t = 14.5$ cm. The total current in each coil amounts to $I = 666.7$ kA . In the numerical calculations each coil is modelled by 2 current loops with a radius $a_t = 68.6$ cm at a spacing $\tilde{h}_t = 7.25$ cm . The toroidal coordinate of the first coil is $\varphi = 11.25^o$. The coils are located at equal toroidal distances of $\delta\varphi = 22.5^o$ along the circular axis of the vacuum chamber, which has a major radius $R_o = 170$ cm , and a minor radius of $a_c = 34$ cm . The toroidal field coils create an average field $B_{\varphi,t} = 12.5$ kG at R_o .

Helical Magnetic Field Coils

The helical magnetic field with $M = 4$ periods along the torus circumference and predominant $\ell = 2$ symmetry is created by the two helical windings (= 'poles') HF-1 and HF-2 , where each pole is divided into two half-poles. The poloidal angular width of a half pole is $\theta_{hp} = 36^o$, the poloidal angular spacing between adjacent half-poles amounts to 18^o . The outer minor radius of each pole is $a_{h2} = 50$ cm , the inner radius is $a_{h1} = 40$ cm . To simplify the numerical calculations of the magnetic surfaces, an effective minor radius of $a_h = 44.5$ cm is assumed, and each half-pole is modelled by three current filaments which are usually split into 200 segments. The poloidal angular distances of each current filament from the pole center amount to 15, 27, and 30^o , respectively, and remain constant whatever the poloidal position of the pole center is. This is a good approximation when using the following winding law for the pole center :

$$M\varphi = -\ell\,(\theta - \alpha\,sin\theta - \beta\,sin2\theta) \;,$$

where $\alpha = a_h/R_o \approx 0.2618$ for a major radius $R_o = 170$ cm and an effective minor radius of the helical windings $a_h = 44.5$ cm and $\beta = -(\alpha/2)^2 \approx -0.0171$. The negative sign in the pitch of the winding law corresponds to a clockwise rotation of the helical windings when advancing in the positive toroidal direction. This winding law has been foreseen for the actual device URAGAN-2M , see /1/ . The relative poloidal distance

of the two poles varies in the toroidal direction. The pole centers are at $\theta = \pm 90^o$ for toroidal postions $|\varphi_\perp| = \ell(\pi/2 - \alpha)/M = 37.5^o$. At the toroidal position of half field periods, $(\varphi_{1/2} = 45^o)$, the poles move closer together towards the radial inside of the mid-plane and keep a larger opening towards the radial outside direction, as compared to pole distances in a system with an unmodulated curve for the pole center $M\varphi = \ell\theta$.

The current in each of the helical poles is set to a total of 1.6 MA , which creates an averaged toroidal field $B_{\varphi,h} = 7.5$ kG at the major radius $R_o = 170$ cm .

In the present computations we prefer a mathematically positive pitch of the helical windings, i.e. a counter-clockwise winding direction. This can be seen in Figure 2 in perspective views, showing the helical windings and the TF-coil system in the upper part, and a vacuum magnetic surface in the lower part. Negative currents in these helical windings produce a toroidal field in the positive φ-direction. The field of the TF-coils increases the field of the helical windings.

Vertical Magnetic Field Coils

The two systems of vertical field coils are formed by coaxial pairs of ring conductors as shown in Figure 1 . They consist of

- four pairs of compensation windings, VF-1 and VF-8 , VF-2 and VF-7 , VF-3 and VF-6 , VF-4 and VF-5 , which compensate the transverse magnetic field $B_\perp$ from the unidirectional helical winding currents, by the use of oppositely directed currents, i. e. positive currents throughout the calculations of the present report, and of
- two pairs of correction windings C-1 and C-4 , C-2 and C-3 , with positive or negative currents for a more refined control of position and shape of magnetic surfaces as well as of the size of the last closed magnetic surface.

In TABLES 1 and 2 , the coordinates for the centers of these windings are listed.

TABLE 1 : Coordinates of the Compensation Windings VF-1 to VF-8 ; identical currents $I = 400$ kA .

	VF-4	VF-5	VF-3	VF-6	VF-2	VF-7	VF-1	VF-8
R (cm)	276.8	276.8	213.9	213.9	127.9	127.9	75.9	75.9
Z (cm)	59.0	-59.0	94.5	-94.5	94.5	-94.5	59.0	-59.0

The correction windings C-1 to C-4 are situated close to the inner vertical field coil pairs VF-1 and VF-8 as well as to the outer ones VF-4 and VF-5. For convenience identical currents in the correction windings are applied. The polarity of the currents is compatible with the computations given in the present report; several current values are entered in Table 2 . They create a normalized vertical field $B_\perp/B_o$ as listed in the last column, where $B_\perp$ is the resulting transverse correction field at R_o, and $B_o =$

$B_{\varphi,t} + B_{\varphi,h}$ is the averaged total toroidal field at this major radius position. The value of -38.5 kA- in the second row of correction currents applies to the URAGAN-2M Standard Case, and is kept constant in this report.

TABLE 2 : Coordinates and currents of the correction windings C-1 to C-4 , and normalized vertical field.

	C-2	C-3	C-1	C-4	$\lvert B_\perp/B_o \rvert$ %
R (cm)	267.0	267.0	66.6	66.6	
Z (cm)	58.0	-58.0	58.0	-58.0	
J (kA)	-103.8	-103.8	-103.8	-103.8	4.5
J (kA)	-38.5	-38.5	-38.5	-38.5	2.8
J (kA)	0.0	0.0	0.0	0.0	1.8
J (kA)	11.5	11.5	11.5	11.5	1.5
J (kA)	69.2	69.2	69.2	69.2	0.0

Magnetic Configurations of the URAGAN-2M Torsatron

Depending on the current ratios in the above four coil systems of the URAGAN-2M torsatron, the size of the outer closed magnetic surface, and the radial profiles of the rotational transform, ι , and of the specific magnetic volume, $V'/V'(0)$, are changed . This can be seen in the bottom traces of Figure 3 . The upper and middle parts of the figure are the magnetic surfaces, the position of the half-poles of the helical windings, and the cross-section of the vacuum chamber, at toroidal angles of 45^o and zero, respectively.

Normalized correction fields $B_\perp/B_o$ between 0 and 4.5 % are applied in this calculation. For convenient classification of other configurations, the parameter $K_\varphi = B_{\varphi,h}/B_o$ is used, where $B_{\varphi,h}$ is the toroidal field component of the helical windings at R_o , and $B_o = B_{\varphi,t} + B_{\varphi,h}$ is defined above. In Figure 3, the value of K_φ amounts to 0.375 ; the correction fields yield $B_\perp/B_o = 2.8\%$ for the Standard Case of URAGAN-2M , at currents of -1.6 MA in the helical windings, 400 kA in the compensation windings, and 666.7 kA in each of the 16 TF-coils. For these data, the outer closed magnetic surface fits the vacuum chamber and is located symmetrically to it at $\varphi = 45^o$. The variation of the magnetic axis position with the value of the correction fields is smaller at $\varphi = 0$ than at 1/2 of the field period. The characteristic resonance $\iota = 1/2$ is avoided in the Standard Case; it is within the ι-profile at lower normalized correction fields of 0 and 1.5 % . Reducing both the correction field and the value of K_φ results in configurations with lower aspect ratio and lower values of the rotational transform and the shear /2/ , compared to those of the Standard Case.

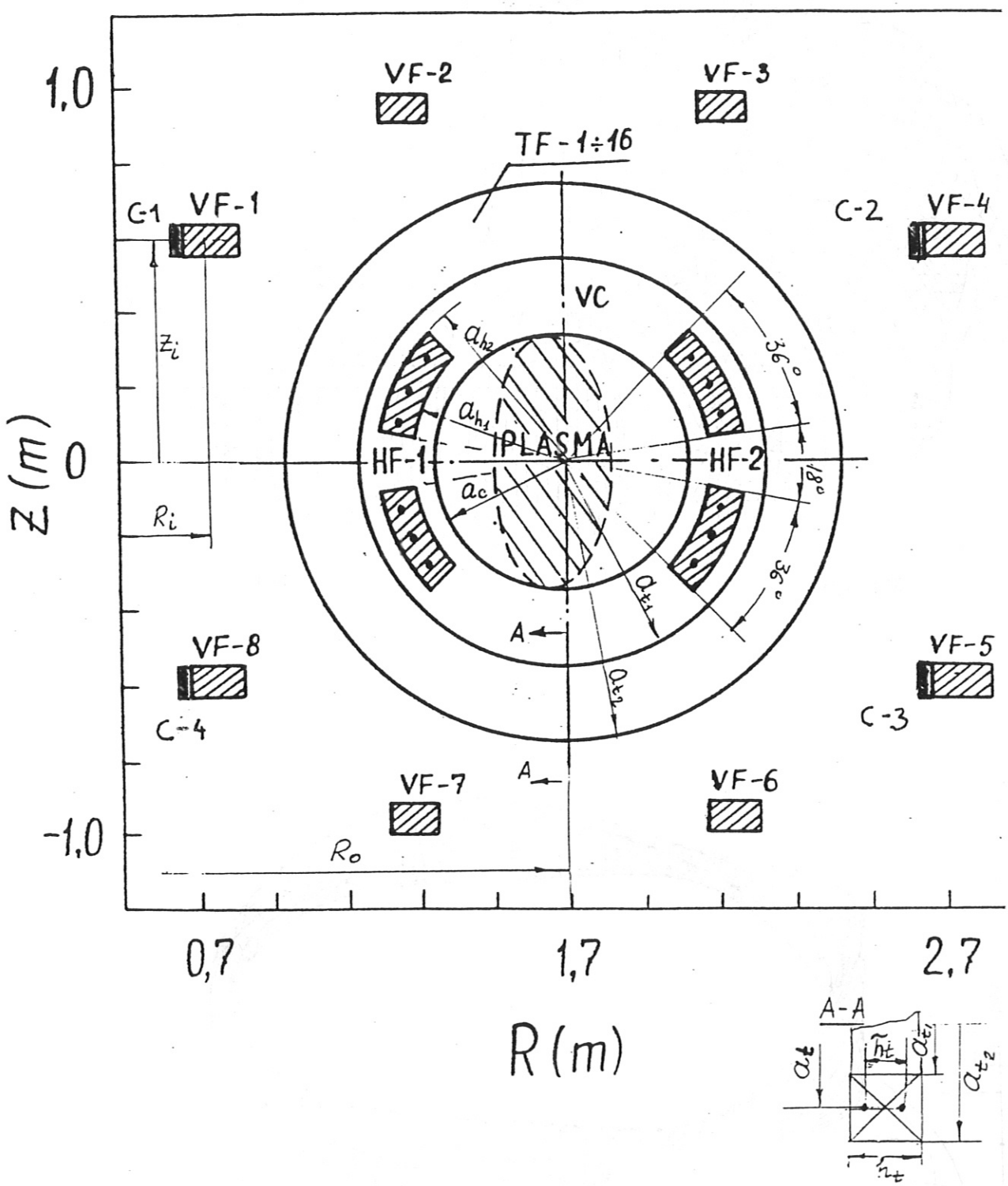

Fig. 1 : Coil systems of URAGAN-2M .

Рис.1

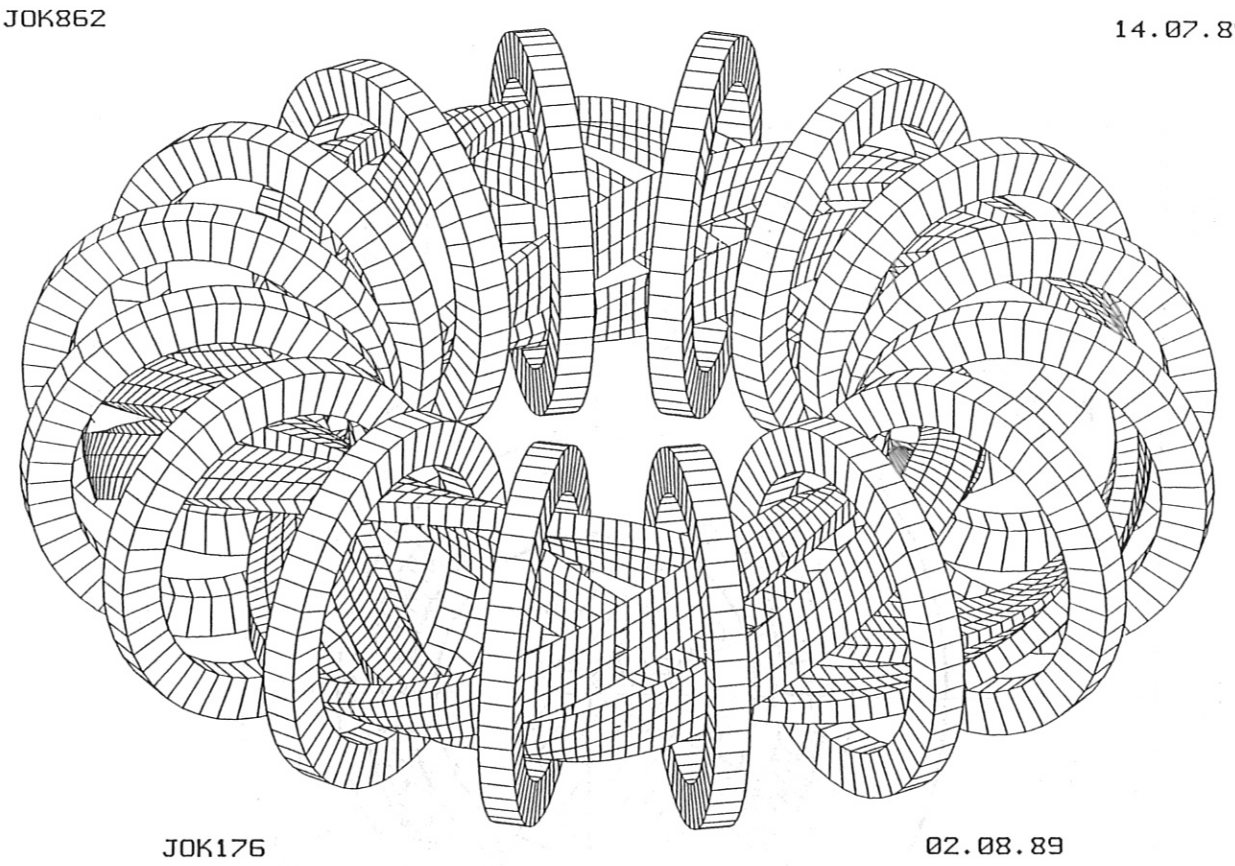

Fig. 2 : Helical windings and TF-coil system,
pitch direction as used in this report (upper part);
Vacuum magnetic surface (lower part).

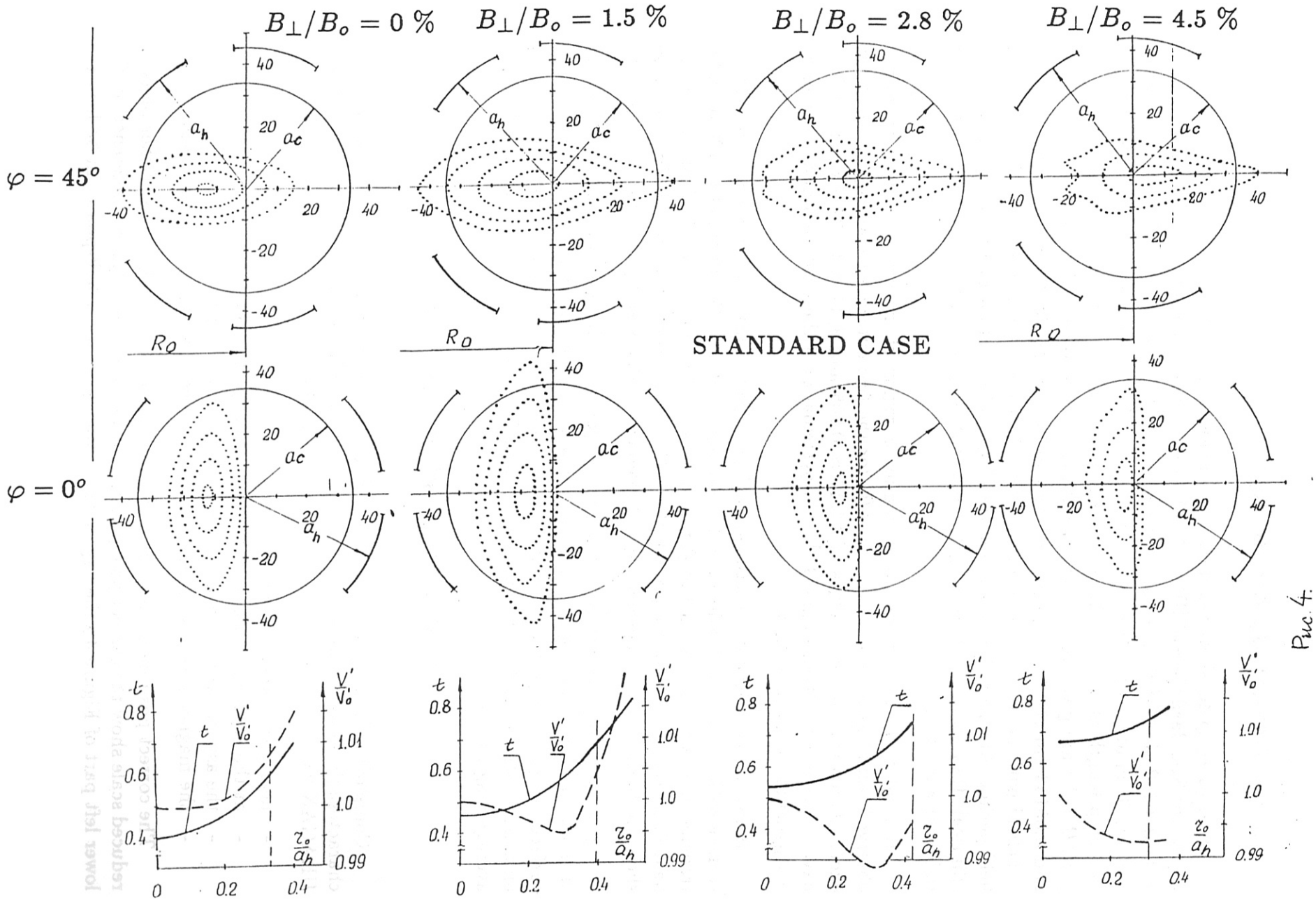

Рис. 4.

Fig. 3 : Influence of correction fields in URAGAN-2M .

3.) URAGAN-2M STANDARD CASE

Figures 4a to 4c show one of the vacuum field calculations performed at IPP Garching for the Standard Case of URAGAN-2M in the three typical toroidal positions of zero, 1/4, and 1/2 of the field period. A group of 15 field lines is started between $R = 164.1$ and 171.3 cm at $\varphi = 0$. Between 5 and 35 toroidal transits are followed at an integration step length of 3 cm . The numerical values of the rotational transform ι and of $\oint dl/B = V'$ are given in the lower right part of Figure 4b ; the axis values are 0.561 and 0.05153 cm$\times$G^{-1} , respectively. As can be seen in the figure, the magnetic axis is helical with an amplitude of about 3 cm ; it attains a value of $R = 170$ cm at 1/2 field period. At this toroidal position the shapes of closed magnetic surfaces are nearly elliptical; they show an increasing triangularity at $\varphi = 0$, out to an effective minor radius of $\bar{r} \gtrsim 13$ cm .

Beyond this value of the minor radius, a region of 'natural' magnetic islands is observed, six large ones at $\iota = 2/3 = 4/6$; for the two outermost starting points at the edge, islands associated ι-values of $12/17 \approx 0.705$ and $8/11 \approx 0.727$ are seen, which have values of $V' \approx 0.0501$ cm$\times$G^{-1}. The systematics of these rational numbers will be discussed in the next section.

Between these island structures, slightly ergodic surfaces are seen. An ergodic surface with $\iota \approx 0.7$ is obtained for the starting point $R = 171.42$ cm after 120 toroidal transits, shown in the top part of Figure 5 . In the bottom part of the figure an 'open' field line results for a starting point $R = 171.45$ cm . Several other field lines are also shown in both parts of Figure 5 , closed magnetic surfaces and parts of the 2/3-islands.

A bulged magnetic surface inside the 2/3-islands, i.e. between the magnetic surfaces # 9 and # 10 of Figure 4 , is obtained for a starting point at $R = 170.14$ cm . This surface yields $\iota = 0.651$ and an averaged minor radius of 13.5 cm , corresponding to an aspect ratio of 12.6 . The value of V' is 0.0501 cm$\times$G^{-1} . This corresponds to an average magnetic well

$$\delta V'/V' = \big(V'(0) - V'(a)\big)/V'(0) = -2.7\,\%\,.$$

Comparing the magnetic surfaces of Figures 4a to 4c and Figure 5 as well as their characteristic values, ι and V' , to those shown in Figure 3 for the Standard Case of URAGAN-2M , we find that in the present computation :

- nearly the same ι-values are seen,
- at the edge magnetic islands and ergodicity are resolved,
- the aspect ratio of closed surfaces seems to be larger,
- the magnetic well is deeper and the increase of V' at the edge is absent.

The correct position of the four half-poles can be seen in Figure 4a. Other plots at reduced scale show the correct pole positions at the other two planes of reference; in the lower left part of Figure 4b the gap of 18° between the inner half-poles can be located.

Some studies have been made regarding possible numerical effects. A rather weak effect on the rotational transform is seen at the values ι_1 to ι_3 for magnetic surfaces with increasing minor radii, if the number of filaments is varied from 3 to 4, if their longitudinal splitting changed from 200 to 360, and if the more exact value of $\alpha = 44.5/170 = 0.261764$ is replaced by 0.2618 , see TABLE 3 :

TABLE 3 : Variation of numerical parameters of the helical windings .

R_{start}	cm				166.0	168.0	170.0
r	cm				3.7	7.8	12.9
job no.	segments	filaments	α-value	transits	ι_1	ι_2	ι_3
FFR056	200	3	0.261764	8	0.5653	0.5841	0.6407
FFR062	200	3	0.261764	15	0.5640	0.5826	0.6393
FFR064	200	2	0.261764	15	0.5730	0.5949	0.6670
FFR066	200	4	0.261764	15	0.5608	0.5782	0.6307
FFR072	200	3	0.2618	10	0.5646	0.5830	0.6380
FFR073	360	3	0.2618	10	0.5642	0.5825	0.6352

In the first row of the table, 8 toroidal transits are followed with a step size of 5 cm . The transit numbers are 10 or 15 in the other tests; the integration step is always 3 cm . The poloidal positions of the cases with 2 and 4 filaments per half-pole are adjusted to the overall poloidal half-pole extension of 36° by setting the filaments to ±18 and 36° at $\varphi = 0$ in the first case, and to ±13.5, 22.5, 31.5, and 40.5° in the second case, and by adjusting the individual currents for a total of 1.6 MA per pole.

The calculation with 2 filaments per half-pole yields ι-values which are larger than the average of the other calculations; the third surface is already a part of the 2/3-islands. The general result is that at higher numerical resolution slightly smaller values are seen for the rotational transform. The influence of the assumed radial position $a_h = 44.5$ cm on the result is discussed in the next section.

(4a)

Fig. 4a to 4c : Standard case of URAGAN-2M as computed at IPP-Garching . 31.07.89

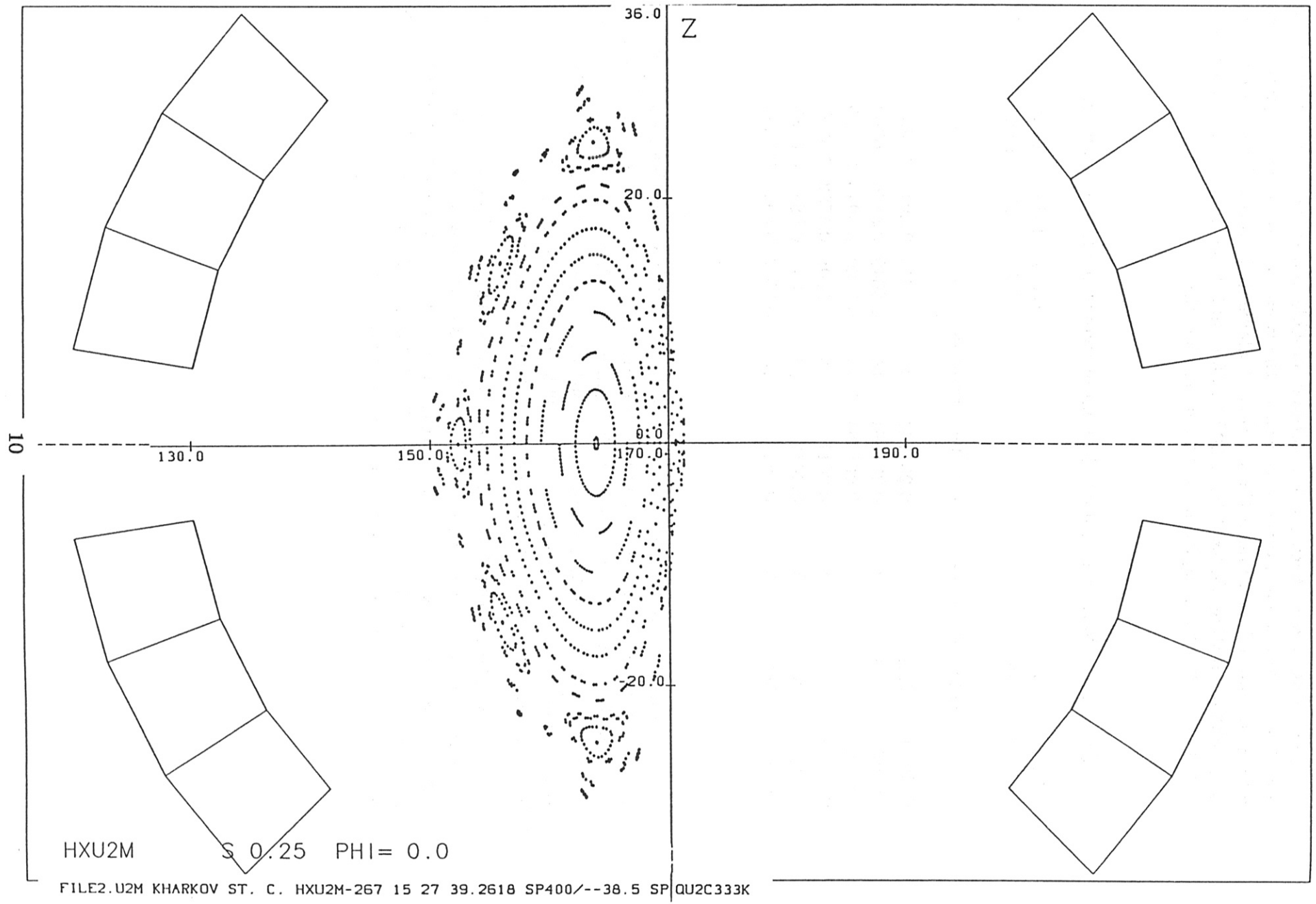

46

FFR121 JOK953 24.07.89 31.07.89

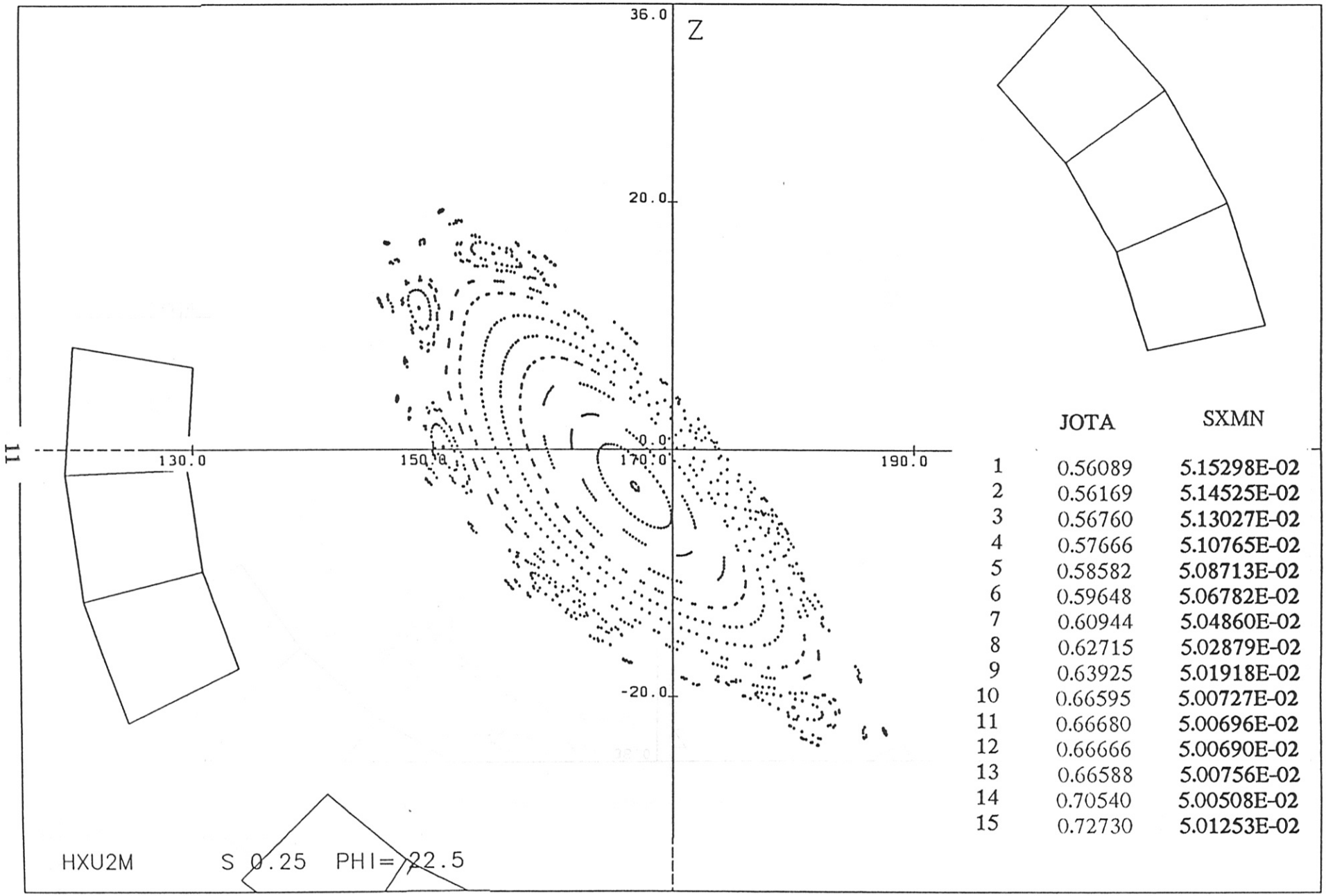

	JOTA	SXMN
1	0.56089	5.15298E-02
2	0.56169	5.14525E-02
3	0.56760	5.13027E-02
4	0.57666	5.10765E-02
5	0.58582	5.08713E-02
6	0.59648	5.06782E-02
7	0.60944	5.04860E-02
8	0.62715	5.02879E-02
9	0.63925	5.01918E-02
10	0.66595	5.00727E-02
11	0.66680	5.00696E-02
12	0.66666	5.00690E-02
13	0.66588	5.00756E-02
14	0.70540	5.00508E-02
15	0.72730	5.01253E-02

4c

FFR121 JOK954

24.07.89 31.07.89

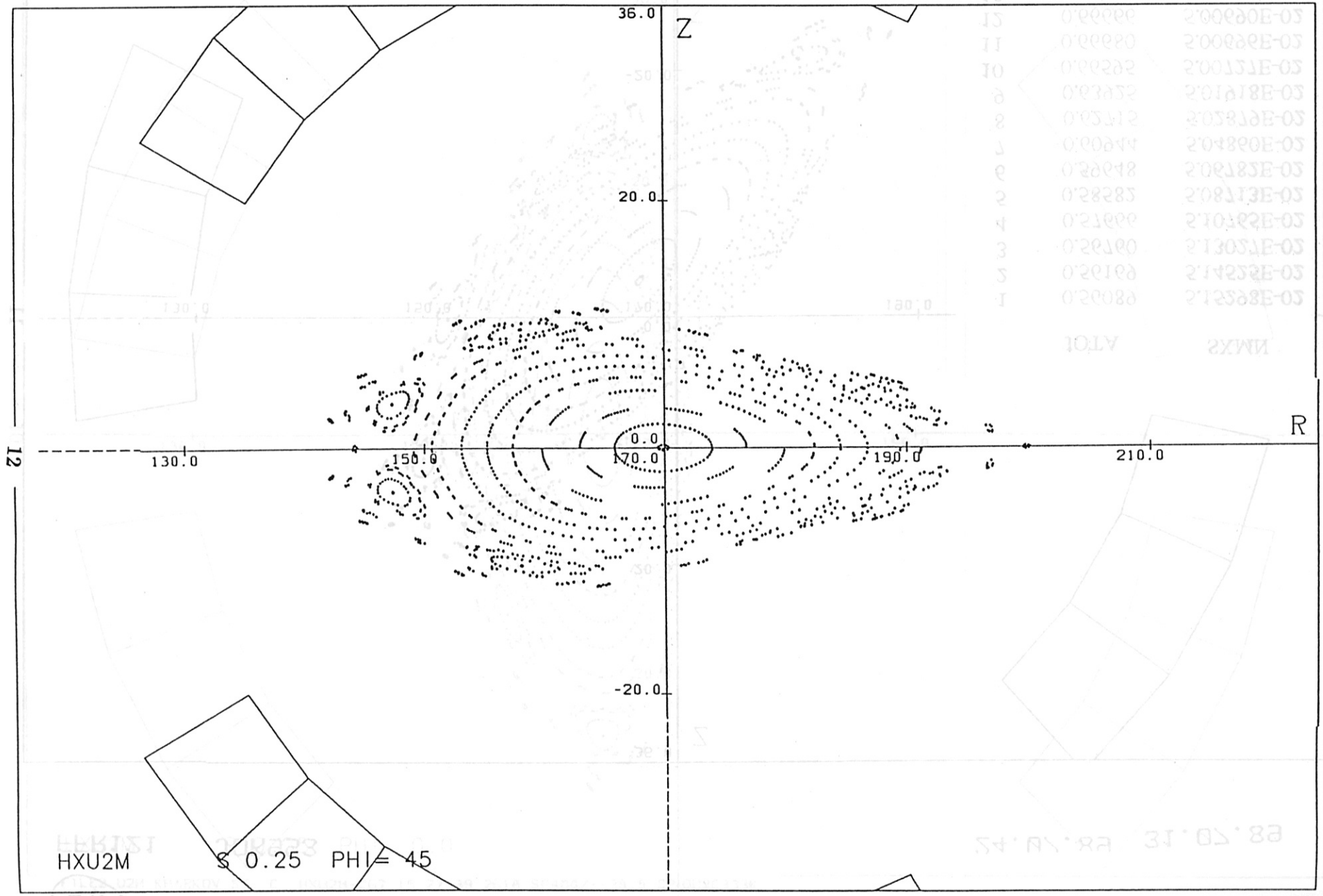

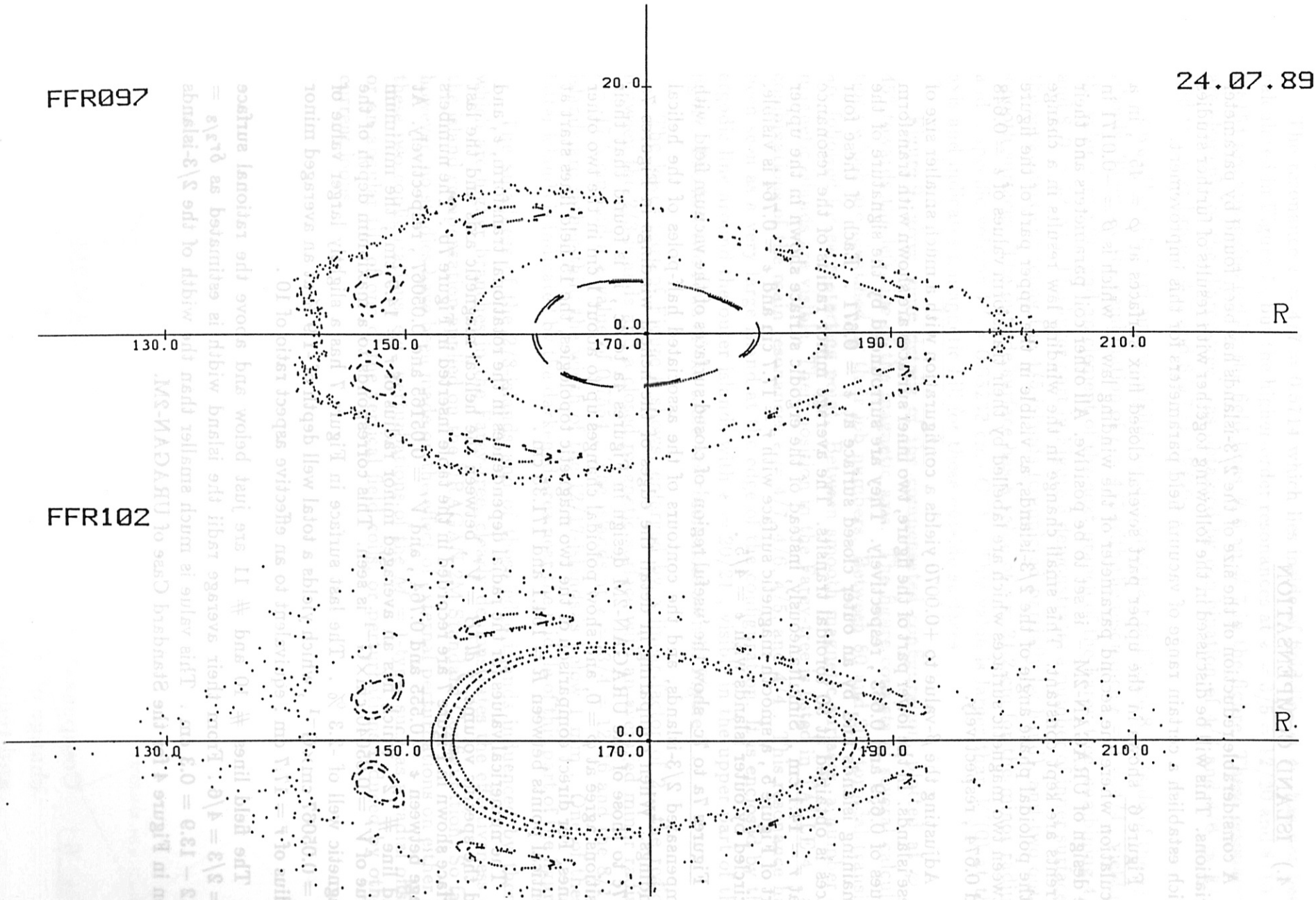

Fig. 5 : Ergodicity at the edge of the configuration (top) and open field line (bottom part) .

4.) ISLAND COMPENSATION

A considerable reduction of the size of the 2/3-islands has been found by parameter variations. This will be discussed in the following together with results of further studies which establish a certain range of vacuum field parameters for this improvement.

Figure 6 shows in the upper part several closed flux surfaces at $\varphi = 45^o$, in a calculation where the second parameter of the winding law – which is $\beta = -0.0171$ in the design of URAGAN-2M – is set to be positive. All other coil parameters and their currents are kept constant. This small change in the winding law results in a change of the poloidal phase angle of the 2/3-islands, as visible in the upper part of the figure between two magnetic surfaces which are labelled by their transform values of $\iota = 0.648$ and 0.674 , respectively.

Adjusting the β-value to +0.0070 yields a configuration with a much smaller size of these islands. In the lower part of the figure, two inner surfaces are shown with transform values of 0.659 and 0.663 , respectively. They are surrounded by the signature of the remaining islands and by an outer closed surface at $\iota = 0.671$. Each of these four traces is obtained at 50 toroidal transits. The average minor radius of the resonance is at $\bar{r} = 14.1$ cm . Simultaneously, instead of the ergodic surface shown in the upper part of Figure 5 , a smooth magnetic surface with $\bar{r} = 17.7$ cm and $\iota = 0.764$ is visible, encircled by outer islands with $\iota = 4/5$.

Figures 7a to 7c show the 'useful region' of closed surfaces of the vacuum field with compensated 2/3-islands, and the contours of the associated half-poles of the helical windings. When comparing in detail the edges of the helical windings in Figures 7a to 7c to those of the URAGAN-2M design in Figures 4a to 4c , it is found that their positions agree at $\varphi = 0$, and show poloidal changes up to about 1 cm in the two other planes. For direct comparison of the two magnetic topologies, the 15 field lines start at identical points between $R = 164.1$ and 171.35 cm .

The numerical values for the radial dependences in the rotational transform, ι, and and the specific volume, $\oint dl/B = V'$, between the helical magnetic axis and the last surface shown in Figure 7 are recorded in the table inserted in Figure 7b . The numbers range between $\iota = 0.555$ and 0.764 , and $V' = 0.05165$ and 0.05067 , respectively. At field line # 12 , which has an averaged minor radius of $\bar{r} = 14.9$ cm , the minimum value of $V' = 0.05040$ cm$\times$G^{-1} is seen. This corresponds to a maximum depth of the magnetic well of -2.3 % . The last surface in Figure 7 has a slightly larger value of $V' = 0.05067$ cm$\times$G^{-1} , which yields a total well depth of -1.9 % at an averaged minor radius of $\bar{r} = 17.7$ cm , equivalent to an effective aspect ratio of 10 .

The field lines # 10 and # 11 are just below and above the rational surface $\iota = 2/3 = 4/6$. From their average radii the island width is estimated as $\delta r_{2/3} = 14.2 - 13.9 = 0.3$ cm . This value is much smaller than the width of the 2/3-islands seen in Figure 4 for the Standard Case of URAGAN-2M.

The resonance $\iota = 4/7 = 0.5714$ which lies inside of field line # 4 , has not been calculated in Figure 7 , but the higher-order resonances at $\iota = 3/5 = 12/20$ and $8/13 = 0.6154$ are approximated by the field lines # 6 an # 7 in the figure. These resonances are elements of the 'Farey-tree' , as obtained by combination of 4/7 and 4/6 $\Rightarrow$ 8/13 and the next branch 4/7 and 8/13 $\Rightarrow$ 12/20 .

Two other island chains are visible in the upper part of Figure 8 outside of the 4/5-islands. They are the combination of $\iota = 4/5$ with the resonance $\iota = 1 = 4/4$, yielding the value $\iota = 8/9$, and an element of the next branch of the Farey-tree, combining 4/5 and 8/9 $\Rightarrow$ 12/14 . The lower part in Figure 8 demonstrates a number of inner surfaces, the separatrix encircling the 4/5-islands (completed partially by hand), and two outer smooth surfaces. The outside surface has a value of $\bar{r} = 21.2$ cm for the minor radius, and a specific volume $V' = 0.05232$ cm$\times$G^{-1} . This value is larger than $V'(0)$ at the axis and indicates a magnetic hill for these outside surfaces.

Figure 9 gives more details of the compensated configuration, plotted at $\varphi = 45^o$ towards the left side of the magnetic axis. The figure consists of several calculations which are identified by their job numbers. Between 80 and 200 toroidal transits are followed for each starting point. Between smooth magnetic surfaces, a number of magnetic islands are visible. Their position in the Farey-tree is listed in TABLE 4 , as combinations of the main resonances $\iota = 4/7$, 4/6, 4/5, and 4/4 . This resonance has been seen as a very large island at the edge of the configuration. It is enclosed by the ergodic line around the outer islands with $\iota = 20/21$, visible in the upper part of the figure. The last two rows of the table are resonances seen in Figure 7 .

The lower part of Figure 9 shows, enlarged by a linear factor of 2 , the region between the 2/3-islands and a closed magnetic surface with an averaged minor radius $\bar{r} = 17.5$ cm and a ι-value of 0.7554 . The islands at $\iota = 3/4 = 12/16$ and the 8/11-islands are rather thin; the width of the 12/17-islands is below 1 mm . One of these latter islands is indicated by the darkened area near the middle of this part of the figure.

The smallness of the 2/3-islands and of those edge islands influenced by them, which are higher branches in the Farey-tree, clearly demonstrates the effectiveness of the island compensation applied on the URAGAN-2M Standard Configuration. So far, however, no studies have been made on the effect of external perturbations on either of these two configurations, e.g. perturbations of the $M = 1$-type, such as a radial offset or an angular tilt of one of the vertical field coils, or perturbations induced by other current loops.

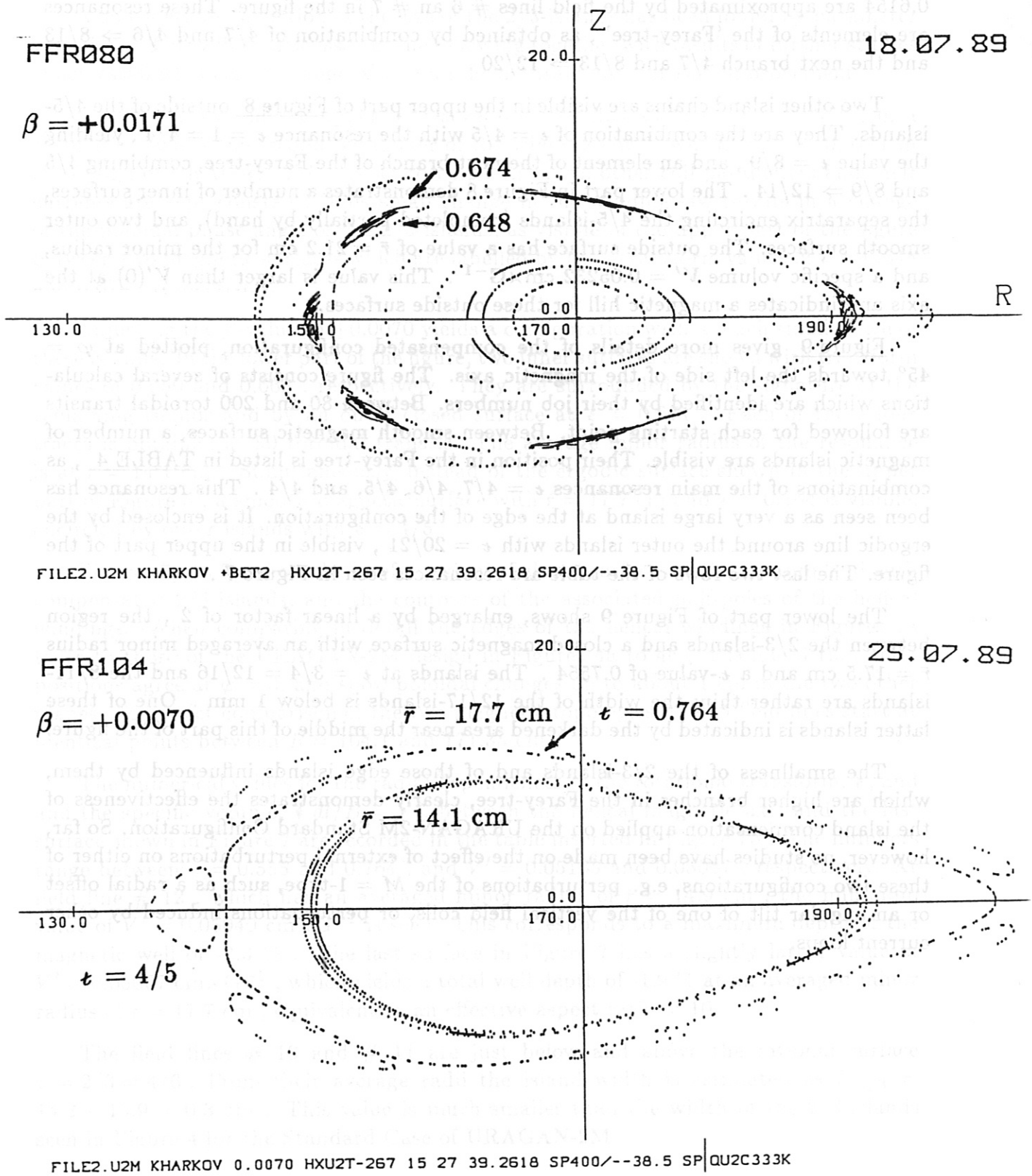

Fig. 6 : Compensation of 2/3-islands in URAGAN-2M
change of poloidal phase of islands (top)
and reduction of island width (bottom part) .

7a

Fig. 7a to 7c : Compensation of 2/3 islands and reduced aspect ratio $A = \approx 10$. magnetic well depth -1.9 % at averaged minor radius of $\bar{r} = 17.7$ cm .

31.07.89

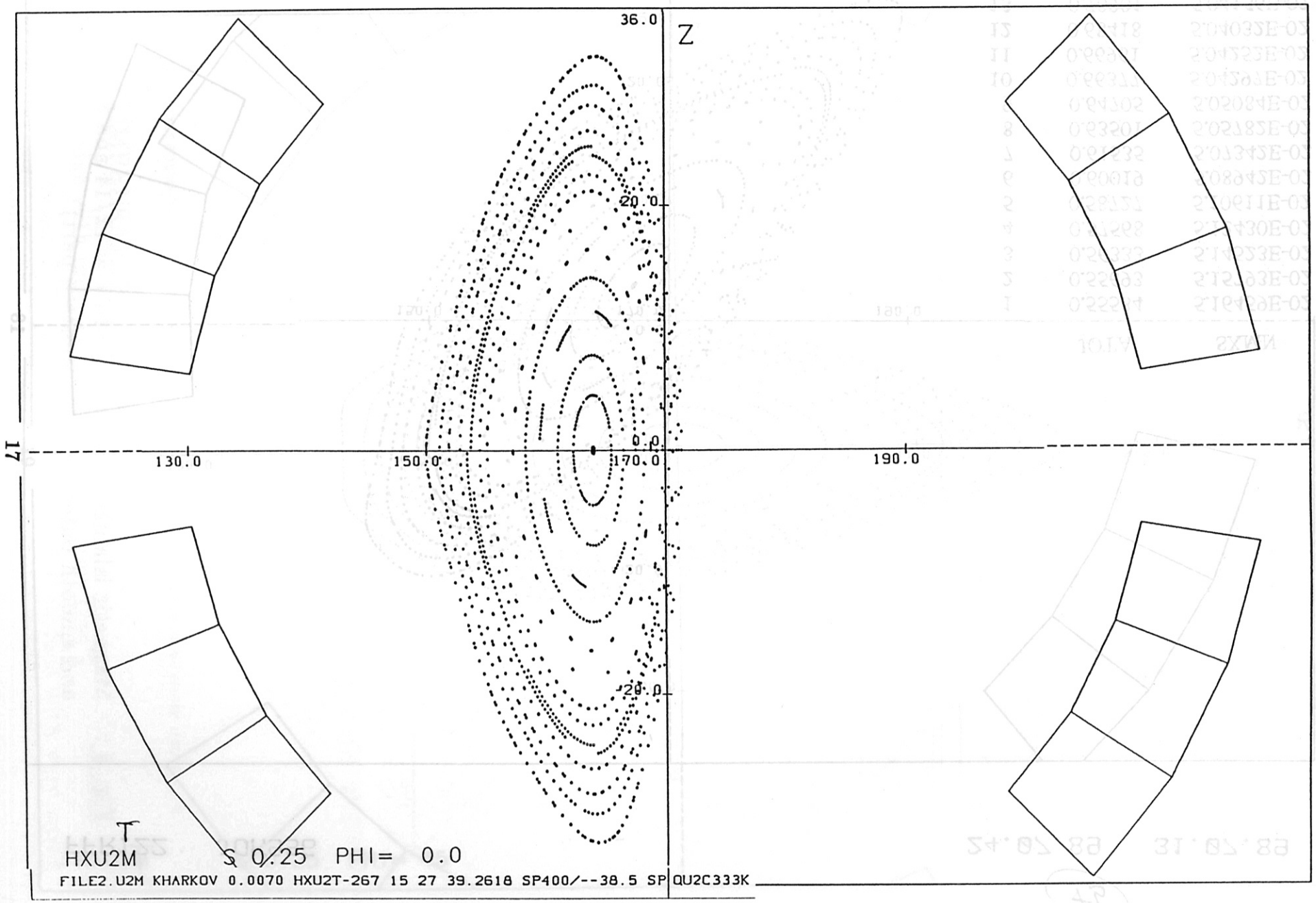

FFR122 JOK956 24.07.89 31.07.89

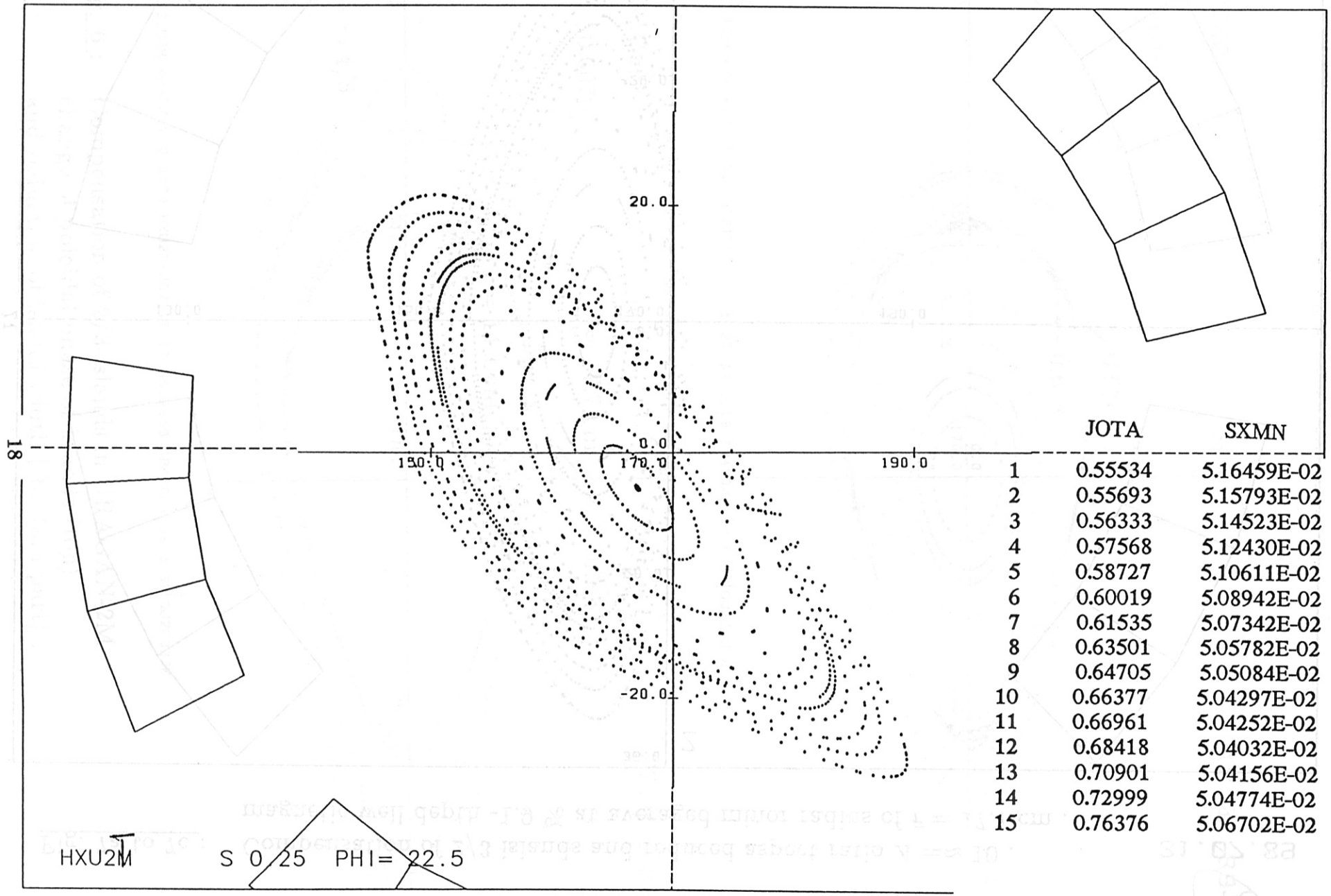

	JOTA	SXMN
1	0.55534	5.16459E-02
2	0.55693	5.15793E-02
3	0.56333	5.14523E-02
4	0.57568	5.12430E-02
5	0.58727	5.10611E-02
6	0.60019	5.08942E-02
7	0.61535	5.07342E-02
8	0.63501	5.05782E-02
9	0.64705	5.05084E-02
10	0.66377	5.04297E-02
11	0.66961	5.04252E-02
12	0.68418	5.04032E-02
13	0.70901	5.04156E-02
14	0.72999	5.04774E-02
15	0.76376	5.06702E-02

FFR122 JOK955

24.07.89 31.07.89

7c

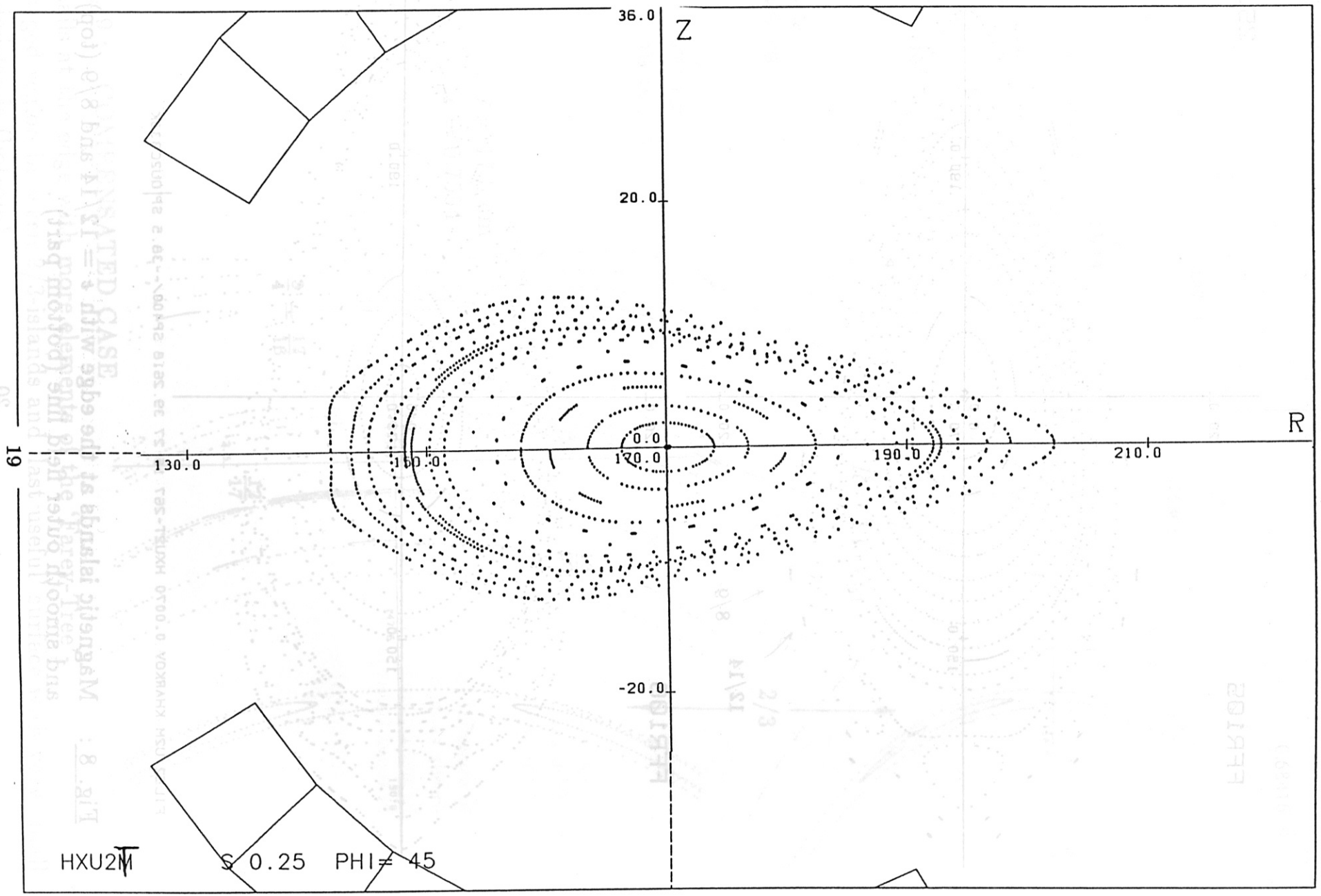

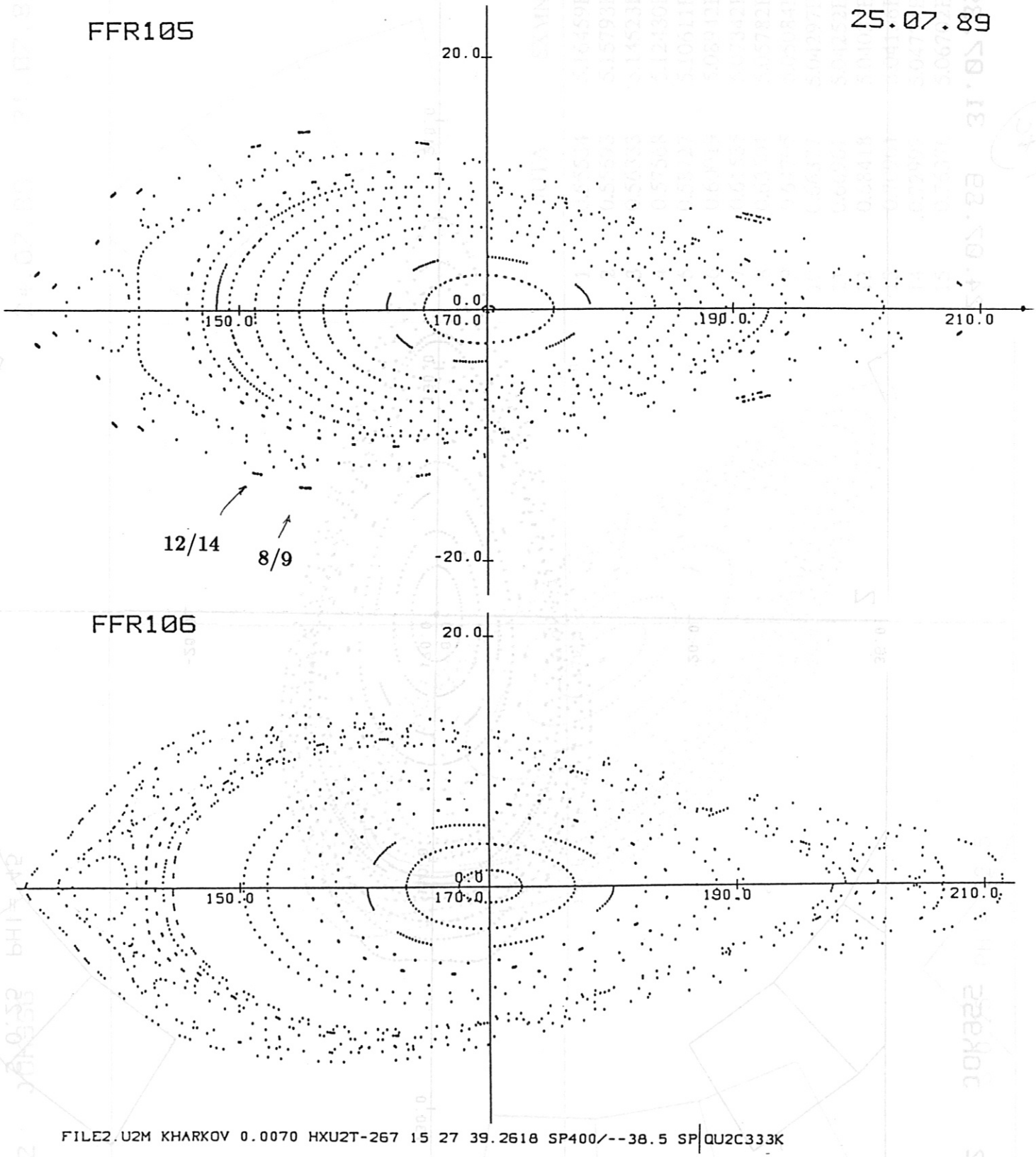

Fig. 8 : Magnetic islands at the edge with $\iota = 12/14$ and $8/9$ (top) and smooth outer field line (bottom part) .

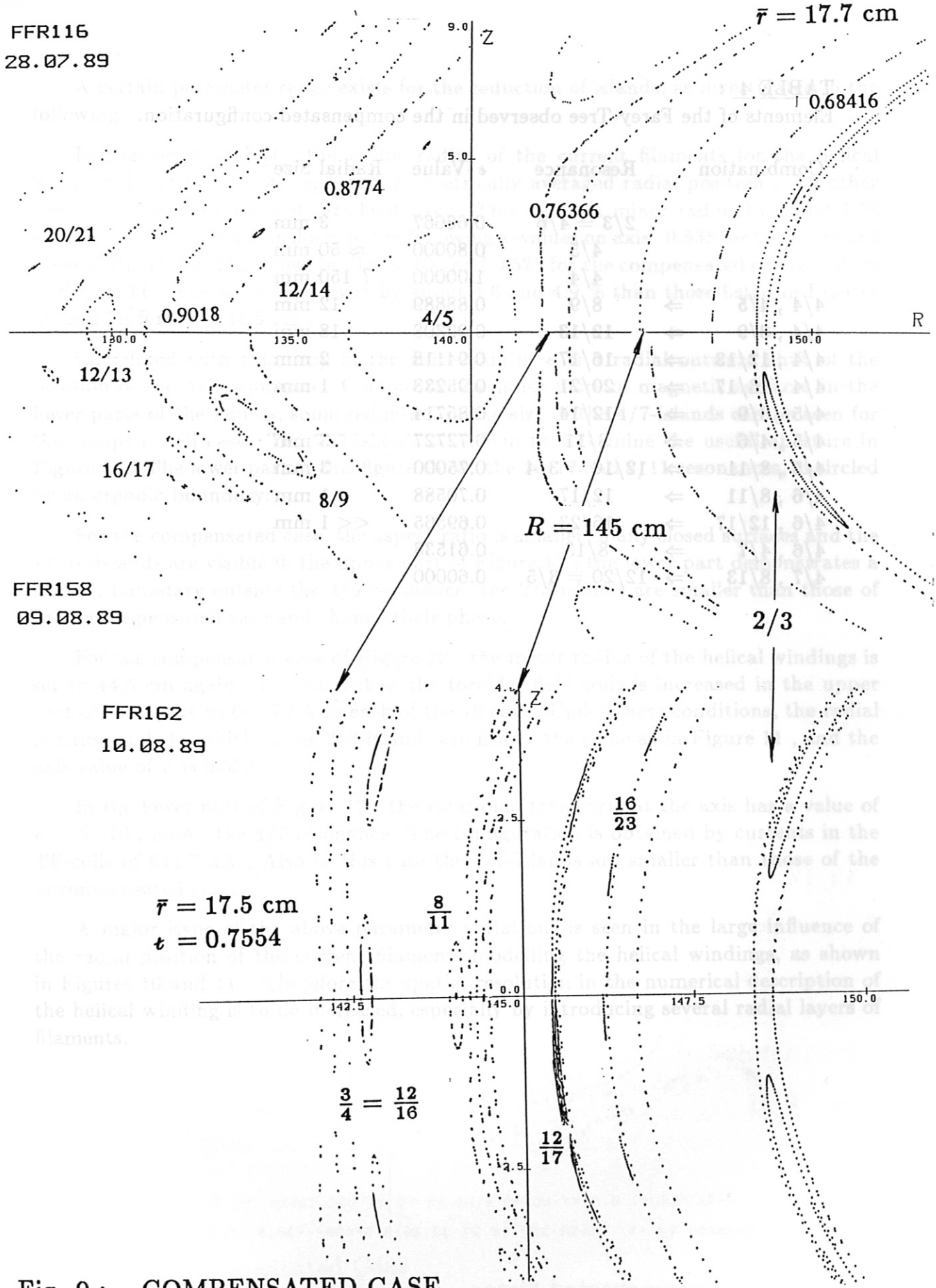

Fig. 9 : COMPENSATED CASE

Details at the edge with more elements of the 'Farey-Tree';
enlarged region between 2/3-islands and 'last useful' surface with very small inside islands (bottom) .

TABLE 4 :
Elements of the Farey-Tree observed in the compensated configuration.

Combination		Resonance	ϵ-Value	Radial Size
		2/3 = 4/6	0.66667	3 mm
		4/5	0.80000	$\approx$ 50 mm
		4/4	1.00000	? 150 mm
4/4 , 4/5	$\Rightarrow$	8/9	0.88889	12 mm
4/4 , 8/9	$\Rightarrow$	12/13	0.92308	18 mm
4/4 , 12/13	$\Rightarrow$	16/17	0.94118	2 mm
4/4 , 16/17	$\Rightarrow$	20/21	0.95238	1 mm
4/5 , 8/9	$\Rightarrow$	12/14	0.85714	
4/5 , 4/6	$\Rightarrow$	8/11	0.72727	3 mm
4/5 , 8/11	$\Rightarrow$	12/16 = 3/4	0.75000	3 mm
4/6 , 8/11	$\Rightarrow$	12/17	0.70588	$<$ 1 mm
4/6 , 12/17	$\Rightarrow$	16/23	0.69565	$<<$ 1 mm
4/6 , 4/7	$\Rightarrow$	8/13	0.61538	
4/7 , 8/13	$\Rightarrow$	12/20 = 3/5	0.60000	

A certain parameter range exists for the reduction of islands, as investigated in the following.

In Figures 10 and 11 , the minor radius of the current filaments for the helical windings is set to $a_c = 45$ cm, their geometrically averaged radial position . All other coil parameters and currents are kept fixed. This offset in minor radius by about 1 % reduces the rotational transform to the following ι-values on axis: 0.535 for the Standard Case of URAGAN-2M shown in Figure 10 , and 0.528 for the compensated configuration of Figure 11 . The values are lower by about 4.6 and 4.9 % than those listed in Figures 4b and 7b for $a_h = 44.5$ cm .

Correlated with this drop in the axis value of ι is a radial outward shift of the position of the 4/7-resonance. Comparing the inner pairs of magnetic surfaces in the lower parts of the figures, some reduction of the size of the 4/7-islands can be seen for the compensated case. The 2/3-islands still seem to determine the useful aperture in Figure 10 . The lower part of this figure shows the 12/17 and 8/11 resonances, encircled by an ergodic boundary.

For the compensated case, the aspect ratio is smaller, many closed surfaces and the 12/16-islands are visible in the upper part of Figure 11 ; the lower part demonstrates a smooth boundary outside the 4/5-resonance: the 2/3-islands are smaller than those of the uncompensated case and change their phase.

For the compensated case of Figure 12 , the minor radius of the helical windings is set to 44.5 cm again. The current in the toroidal field coils is increased in the upper part of the figure to 688.7 kA in each of the 16 coils. Under these conditions, the radial position and the width of the 2/3-islands are nearly the same as in Figure 11 , and the axis value of ι is 0.530 .

In the lower part of Figure 12 , the rotational transform at the axis has a value of $\iota = 0.579$, above the 4/7 resonance. The configuration is obtained by currents in the TF-coils of 644.7 kA . Also in this case the 2/3-islands are smaller than those of the uncompensated case.

A major issue of the above parameter variations is seen in the large influence of the radial position of the current filaments modelling the helical windings, as shown in Figures 10 and 11 . Therefore the spatial resolution in the numerical description of the helical winding is to be increased, especially by introducing several radial layers of filaments.

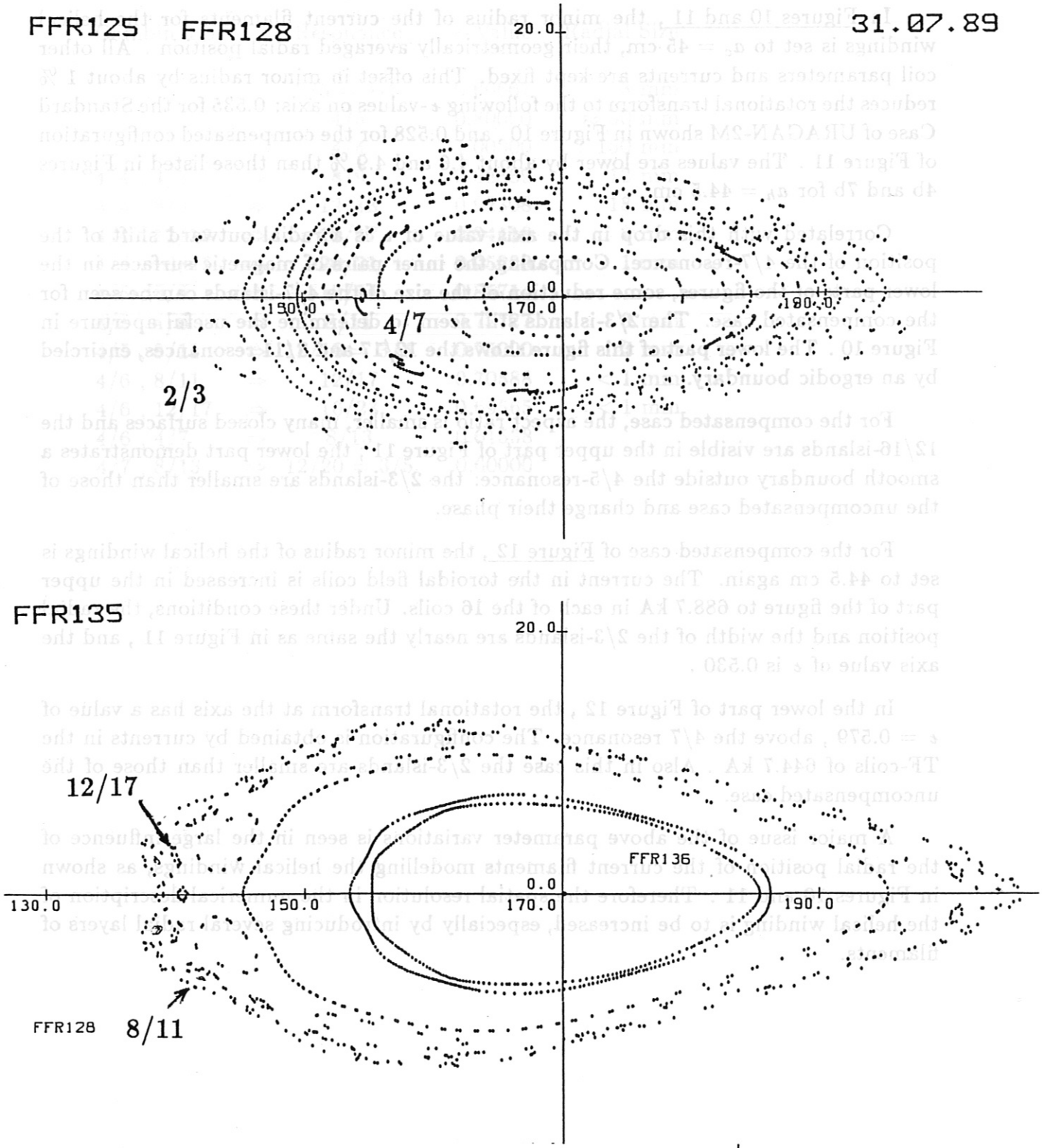

Fig. 10 : Uncompensated Case
Effective minor radius of helical windings 45 cm

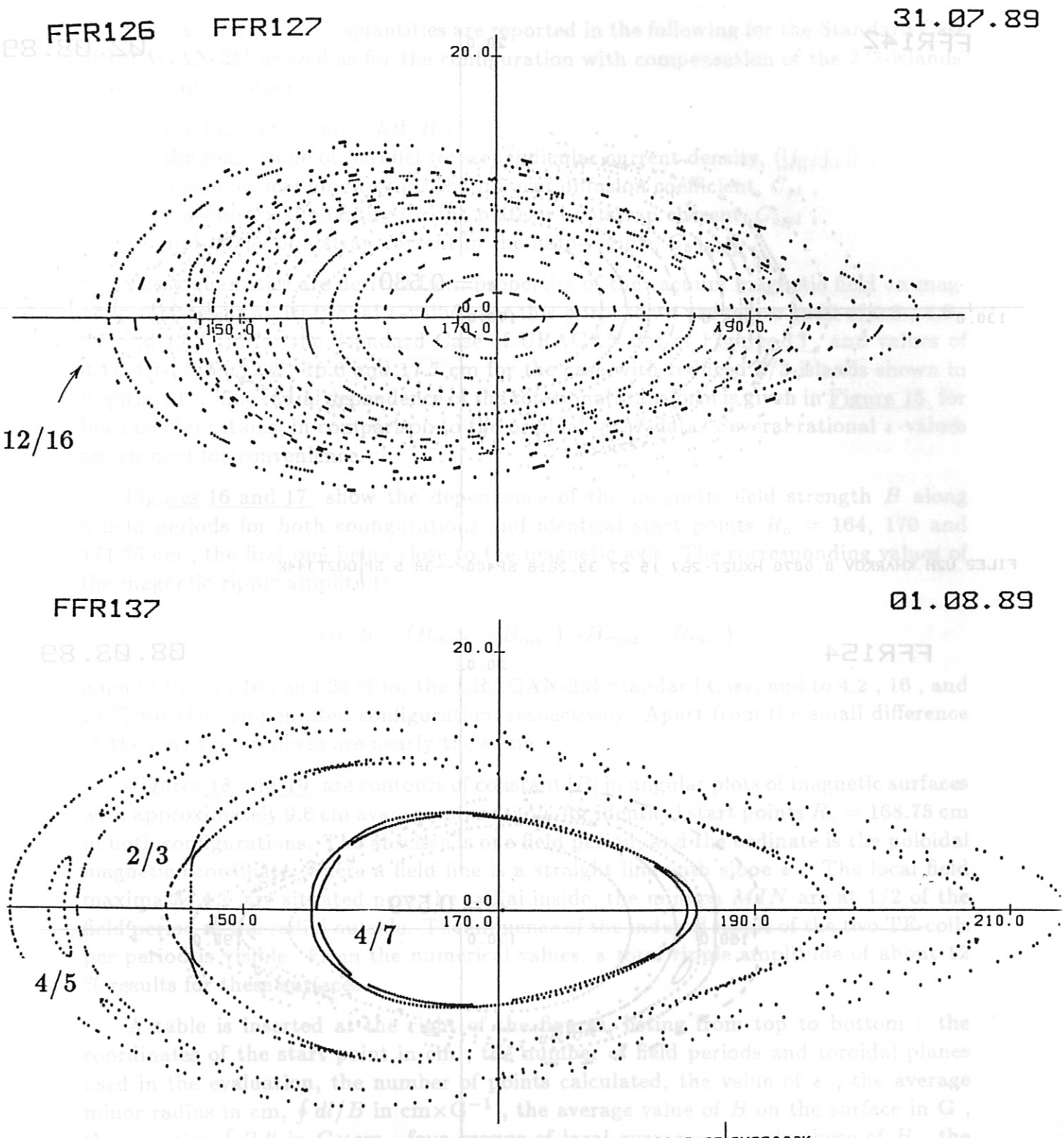

Fig. 11 : Compensated Case
Effective minor radius of helical windings 45 cm

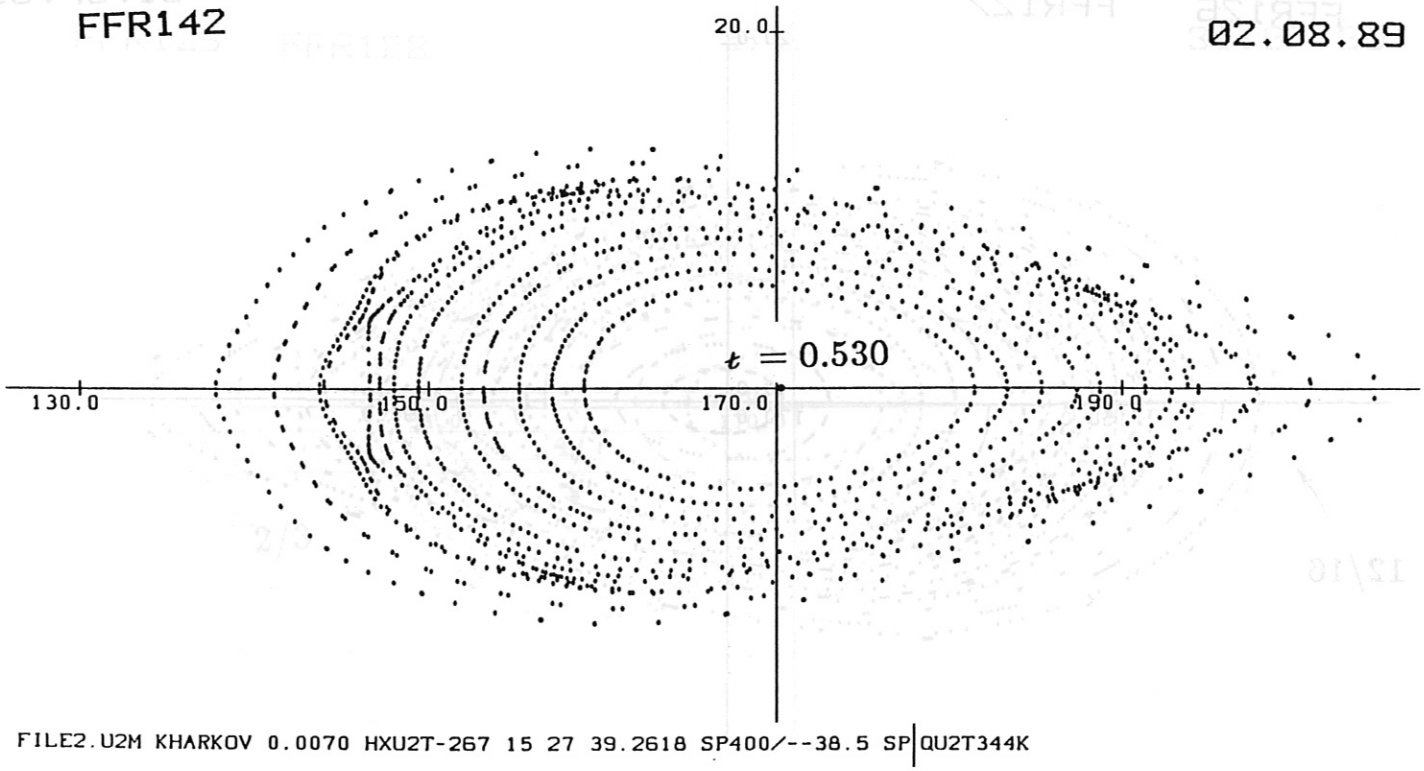

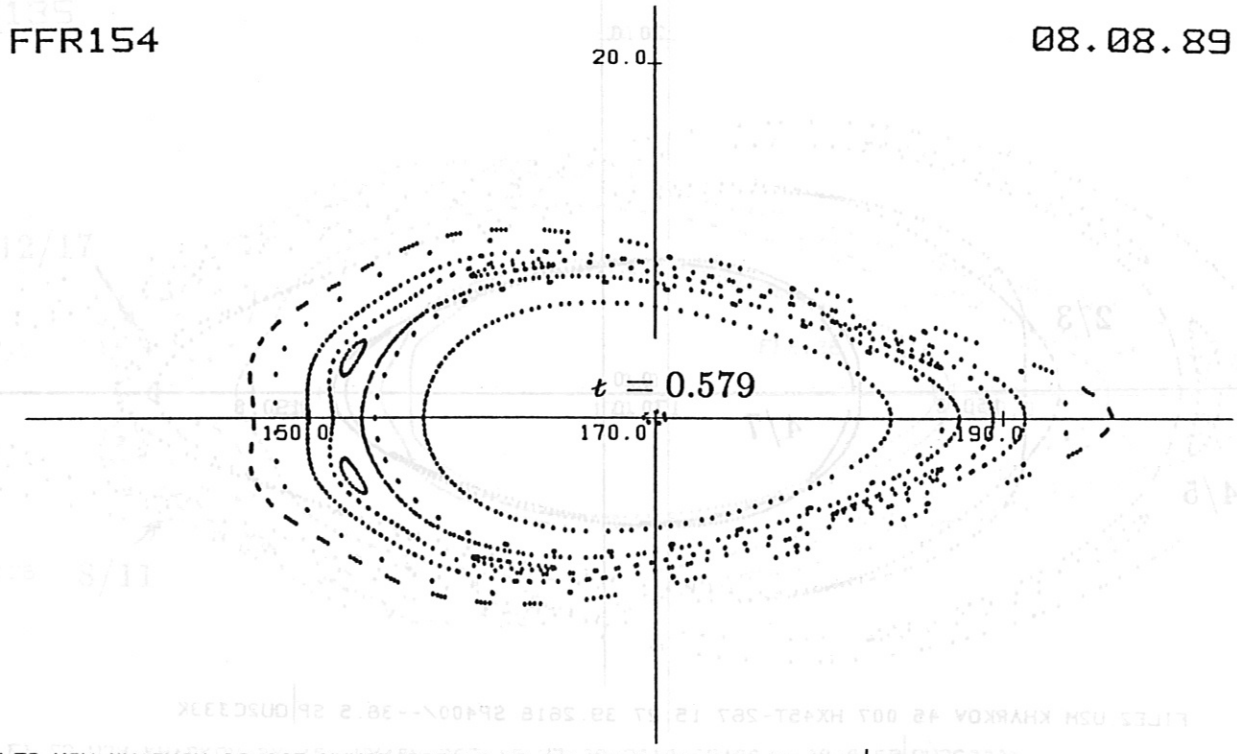

Fig. 12 : Compensated Case
Increased (top) and reduced (bottom) current in TF-Coils

5.) CHARACTERISTIC NUMBERS

Several characteristic quantities are reported in the following for the Standard Case of URAGAN-2M as well as for the configuration with compensation of the 2/3-islands. The relevant numbers are :

- the magnetic ripple, $\delta B/B$,
- the magnitude of parallel to perpendicular current density, $\langle |j_{||}/j_{\perp}| \rangle$,
- a geometrical quantity for the plateau diffusion coefficient, C_{pl} ,
- a geometrical quantity for the plateau bootstrap current, $C_{b,pl}$,
- and of the bootstrap current in the lmfp-regime, $C_{b,lmfp}$.

These quantities are derived from properties of the vacuum magnetic field on magnetic surfaces at an irrational ι-value. For this purpose we use minor radii of 0.5 , 4.6 , 9.5 and 12.2 cm for the Standard Case of URAGAN-2M of Figures 13 , and values of 0.4 , 4.7 , 9.7 , 12.2 , 16.6 and 17.7 cm for the case with reduced 2/3-islands shown in Figures 14 . The radial dependence of the rotational transform is given in Figure 15 for both configurations, in comparison to the original $\mathcal{Y}2M$-data. Several rational ι-values are entered for convenience.

Figures 16 and 17 show the dependence of the magnetic field strength B along 8 field periods for both configurations and identical start points R_o = 164, 170 and 171.35 cm , the first one being close to the magnetic axis. The corresponding values of the magnetic ripple amplitude

$$\delta B/B = (B_{max} - B_{min})/(B_{max} + B_{min})$$

amount to 3.3 , 16 , and 24 % for the URAGAN-2M Standard Case, and to 4.2 , 16 , and 24 % for the compensated configuration, respectively. Apart from the small difference at the axis the numbers are nearly the same.

Figures 18 and 19 are contours of constant $|B|$ in angular plots of magnetic surfaces with approximately 9.6 cm average minor radii, for identical start points R_o = 168.75 cm in both configurations. The abscissa is one field period, and the ordinate is the poloidal magnetic coordinate, where a field line is a straight line with slope ι . The local field maxima MAX are situated near the radial inside, the minima MIN are at 1/2 of the field period at the radial outside. The influence of the induced ripple of the two TF-coils per period is visible. From the numerical values, a total ripple amplitude of about 12 % results for these surfaces.

A table is inserted at the right of the figures, listing from top to bottom : the coordinates of the start point in cm , the number of field periods and toroidal planes used in the evaluation, the number of points calculated, the value of ι , the average minor radius in cm, $\oint dl/B$ in cm$\times$G^{-1} , the average value of B on the surface in G , the quantity $\int Bdl$ in G$\times$cm , four groups of local averages, namely those of B , the maximum and average variations of B and the average variation of $\int dl/B$, these four groups of averages being taken at 0, 1/4, 1/2 and 3/4 of the field period, respectively, and the values of $\langle |j_{||}/j_{\perp}| \rangle$ and of J^* .

The quantity $\langle |j_{||}/j_{\perp}| \rangle$ is the ratio of the parallel and perpendicular current densities, averaged over the flux surface. It is derived from the poloidal variation of $\int dl/B$

taken along one field period. Figures 20 and 21 show the S-shaped current lines of both topologies, overlaid are contours of constant $j_{||}/j_{\perp}$. The minima MIN are deeper than the maxima MAX .

$J^{\star} = \langle (B_o^2/B^2) \cdot (1 + (j_{||}/j_{\perp})^2) \rangle$ enters the stability criterion of resistive interchange modes, and is a direct measure of reduced secondary currents. Values of 8.7 and 7.9 are listed for the two configurations as last entries in the tables. The quantity B_o in the relation of $J^{\star}$ is the average field on the magnetic surface.

In the Figures 22 and 23 the Fourier-coefficients are plotted for the magnetic surfaces of Figures 13 and 14 . The tables inserted in the upper left of Figures 22 and 23 list the first coefficient $A_{(0,0)}$, the effective minor radius in cm , the numerical values of the normalized plateau diffusion and bootstrap coefficients, and identify the symbols used in the plots of the Fourier coefficients.

The quantities C_{pl} and C_b are geometrical factors determining the plateau values for the diffusion coefficient and for the bootstrap current, respectively, normalized to axisymmetric values of an equivalent configuration with the same rotational transform ι and aspect ratio. They are calculated from the Fourier-coefficients of $|B|$ according to a relationship described in /3/ .

The bootstrap current in stellarators for plasmas in the lmfp-regime is studied in ref. /4/ . The numerical result obtained at IPP Garching for the improved case of URAGAN-2M is shown in the lower part of Figure 24 , giving the radial profile of the coefficient of the bootstrap current $C_{b,lmfp}$ in the long mean free path regime, multiplied by f_t/f_c , the ratio of trapped to circulating particles. The normalized number of trapped particles is given in the upper part of the figure.

As a general result for the Standard Case of URAGAN-2M and the compensated configuration we find nearly identical numbers in the tables of Figures 18, 19 and 22, 23 ; for $\langle |j_{||}/j_{\perp}| \rangle$ and $J^{\star}$ a small improvement is seen in the compensated case. Numbers of these characteristic quantities obtained for other classical and advanced stellarators are given in /5/ to /10/ . An example of such a comparison /11/ is shown in Figure 25 , plotting as 'parallel current density' the values of $\langle |j_{||}/j_{\perp}| \rangle$ versus the rotational transform ι . The relationships obtained for URAGAN-2M and the configuration with compensated 2/3-islands are entered in the figure; the results are in the vicinity of data obtained for the W VII-A stellarator and the ATF-torsatron . The relationship $\sqrt{2}/\iota$ applies for the classical stellarator, regarding the average value of $\langle |j_{||}/j_{\perp}| \rangle$ as a function of the rotational transform.

FFR110

JOTA	SXMM	RQA	RQM	A	Q	KL.R
0.55909	5.1529E-02	163.9	169.9	0.7	2.7918E-04	0.5
0.56685	5.1309E-02	163.7	169.5	67.7	2.7954E-04	4.6
0.59645	5.0679E-02	163.1	168.5	286.1	2.7822E-04	9.5
0.62715	5.0288E-02	161.9	168.5	466.8	2.7779E-04	12.2

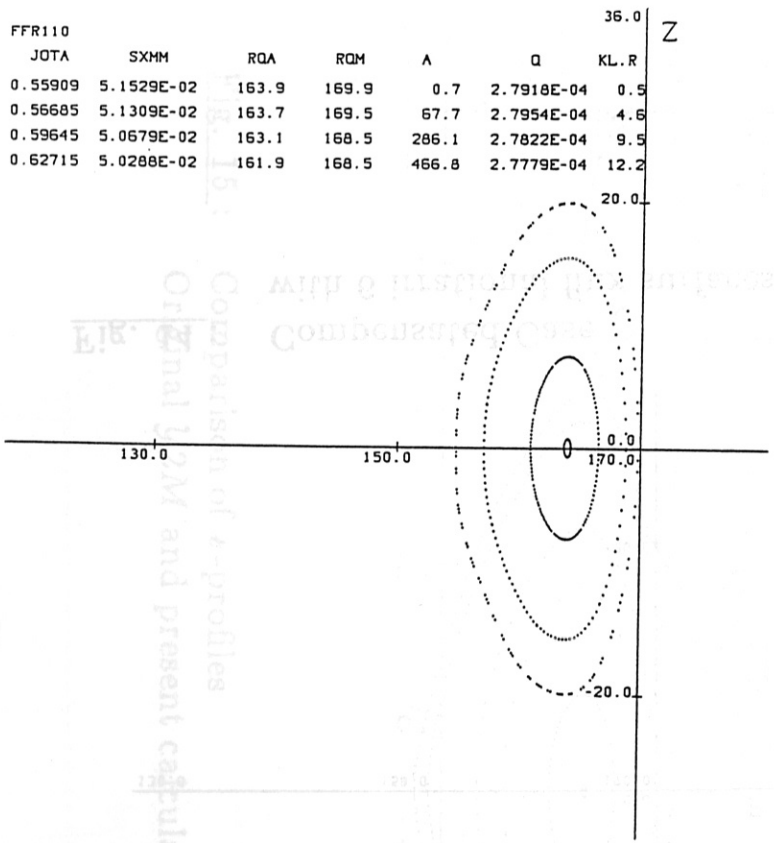

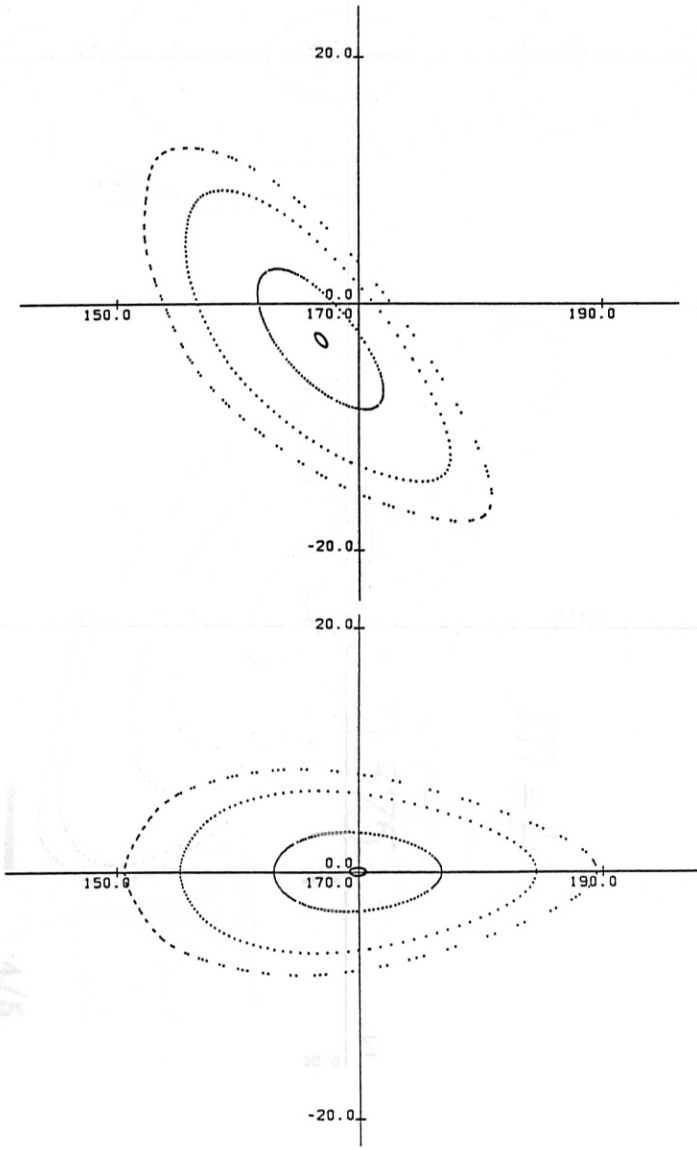

Fig. 13 : URAGAN-2M Standard Case with 4 irrational flux surfaces .

FFR107

JOTA	SXMM	RQA	RQM	A	Q	KL.R
0.55371	5.1645E-02	164.0	170.1	0.4	2.6424E-04	0.4
0.56349	5.1451E-02	163.7	170.2	69.1	2.6427E-04	4.7
0.60019	5.0894E-02	162.8	170.2	293.4	2.6731E-04	9.7
0.63502	5.0578E-02	161.8	170.0	478.7	2.6356E-04	12.3
0.72999	5.0477E-02	161.1	171.2	870.0	2.6991E-04	15.6
0.76376	5.0670E-02	160.7	172.4	981.6	2.8397E-04	17.7

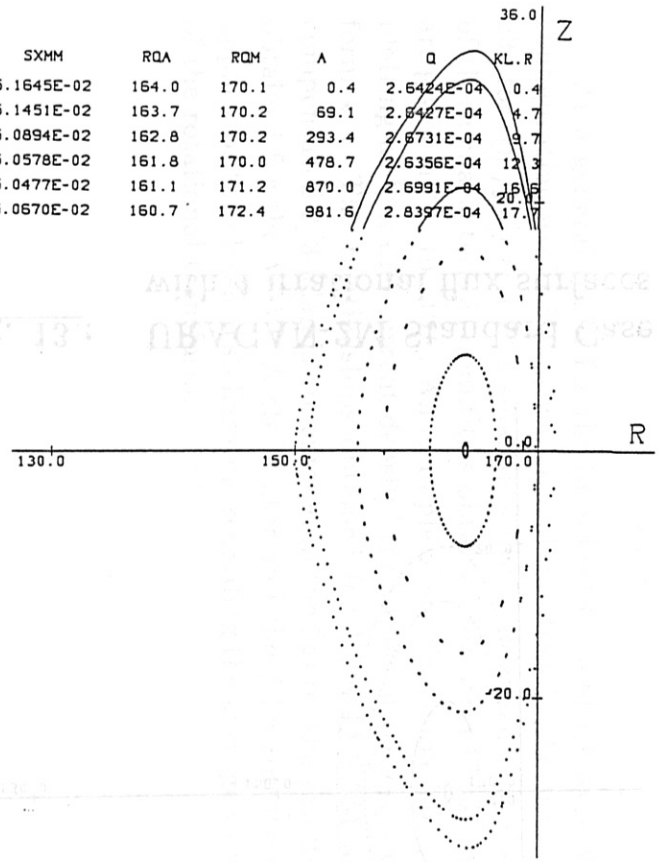

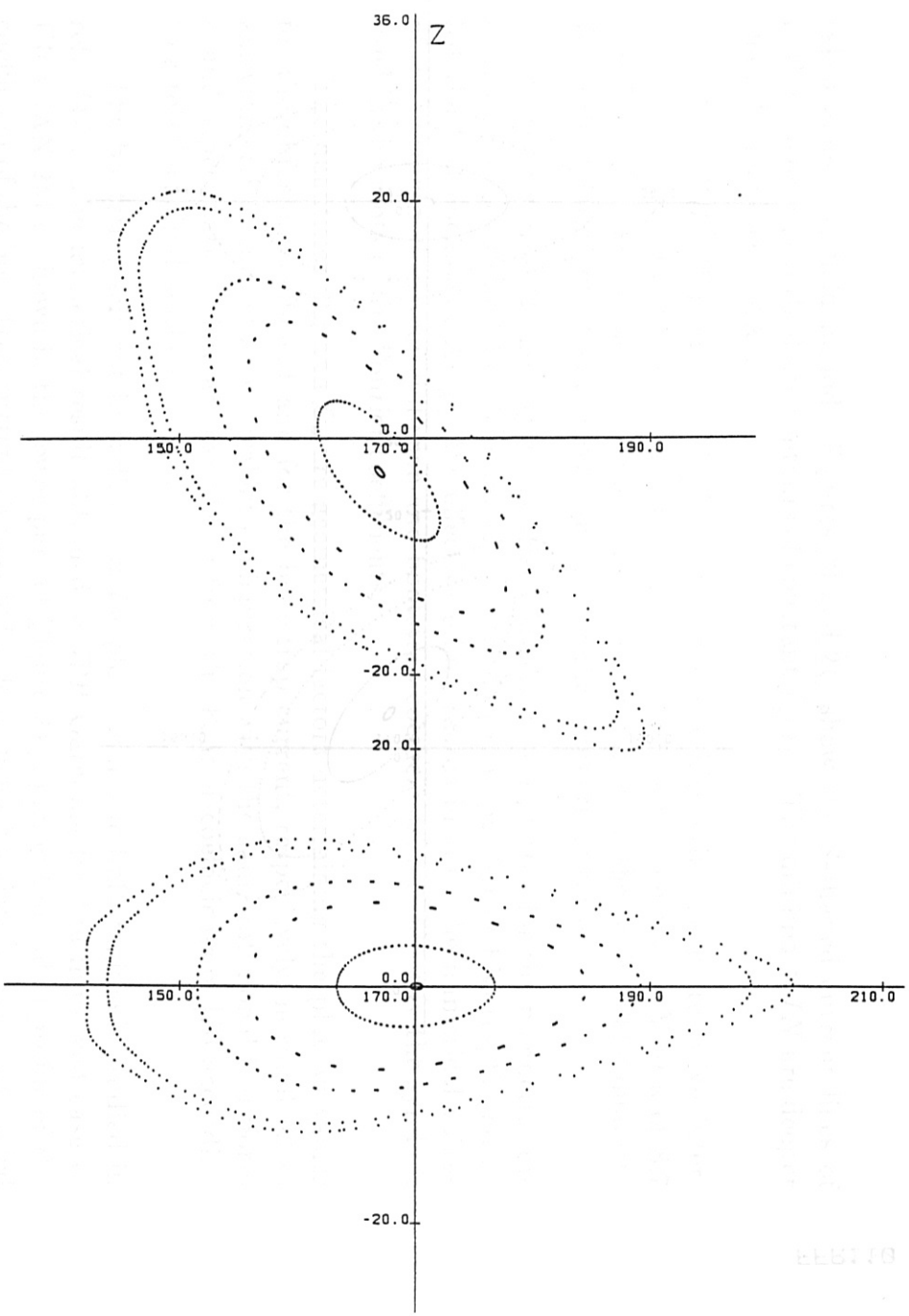

Fig. 14 : Compensated Case with 6 irrational flux surfaces .

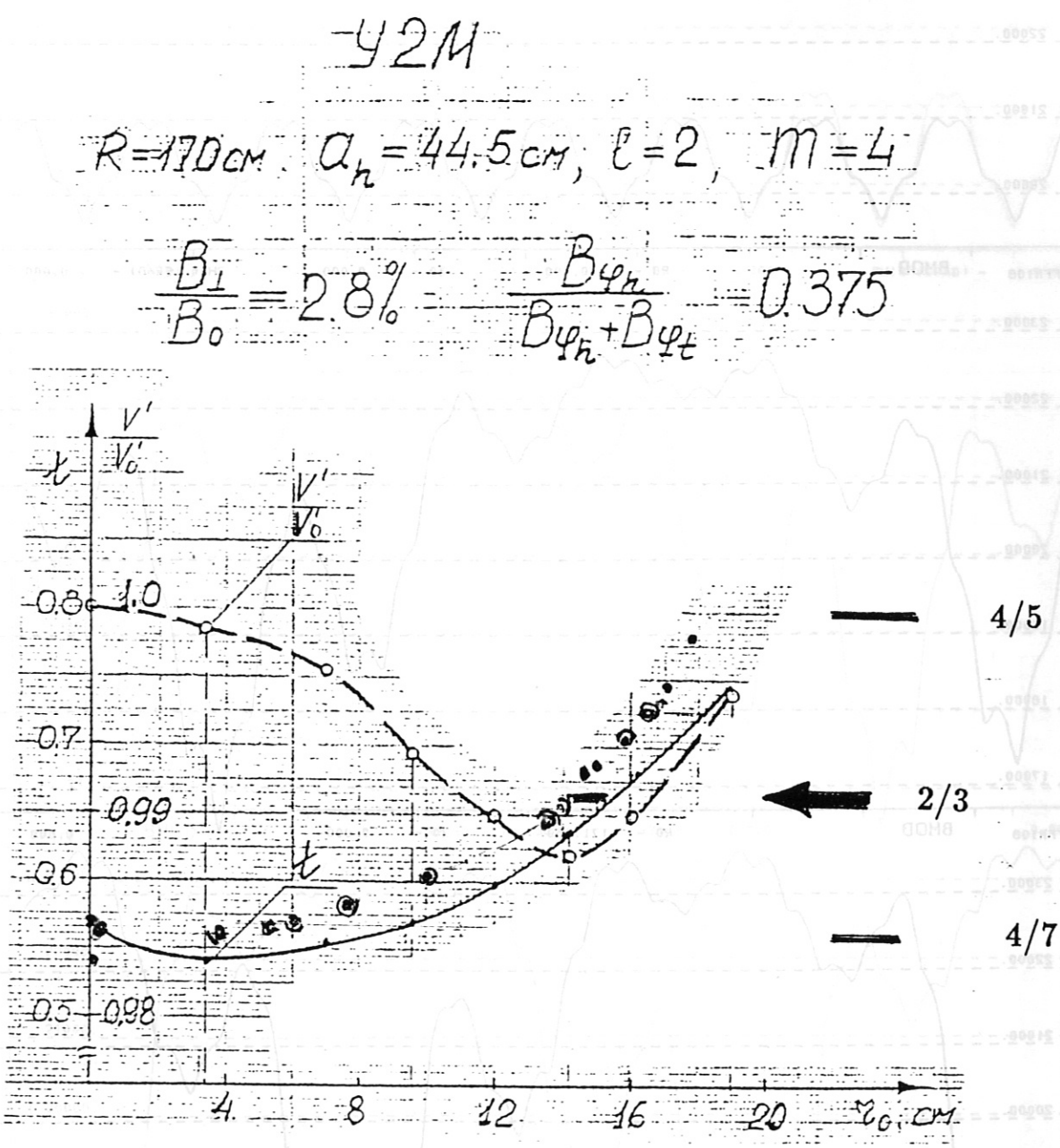

Fig. 15 : Comparison of ι-profiles
Original $y2M$ and present calculations .

25.07.89

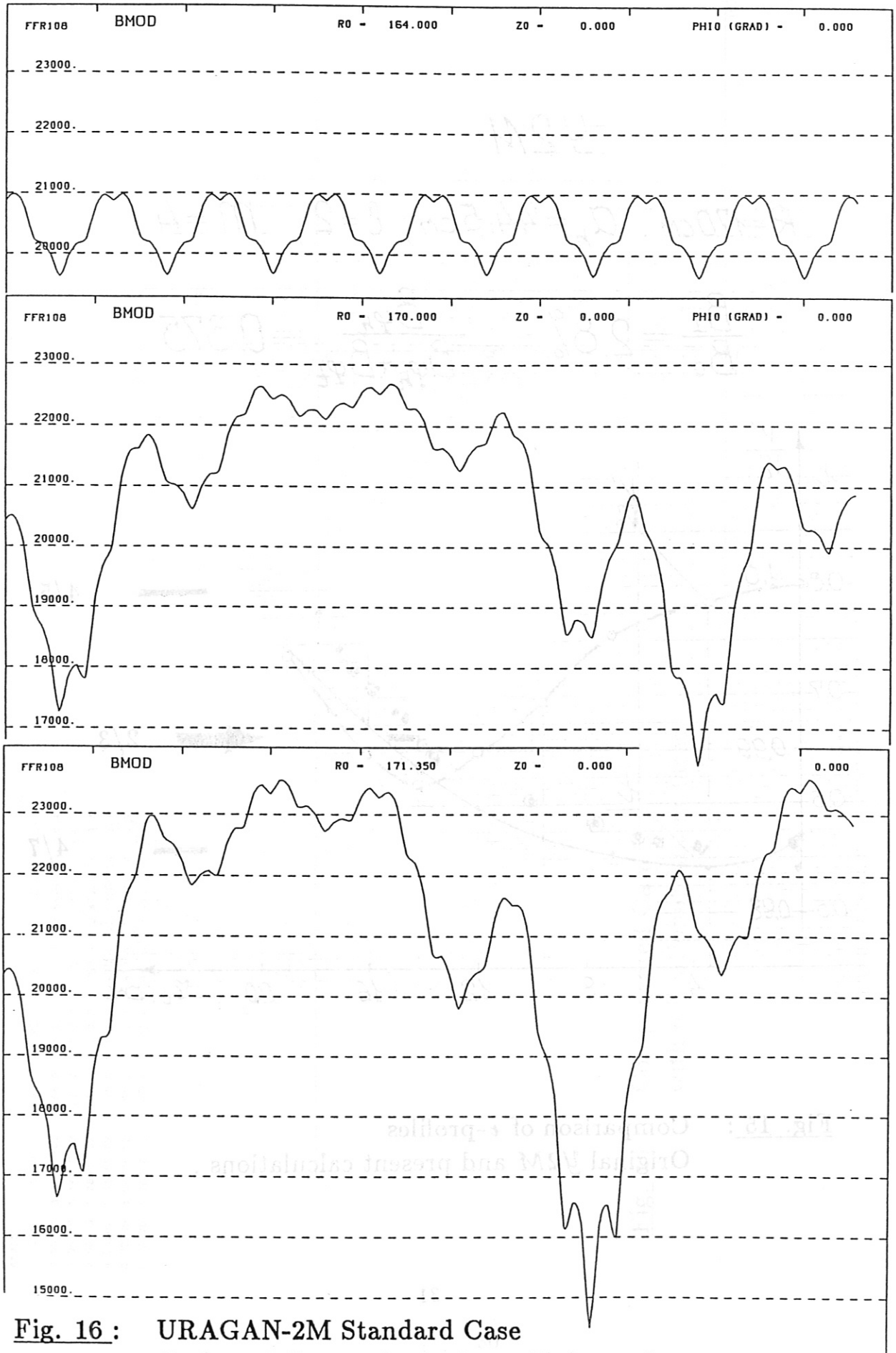

Fig. 16 : URAGAN-2M Standard Case
B along 3 flux surfaces; 2 toroidal transits .

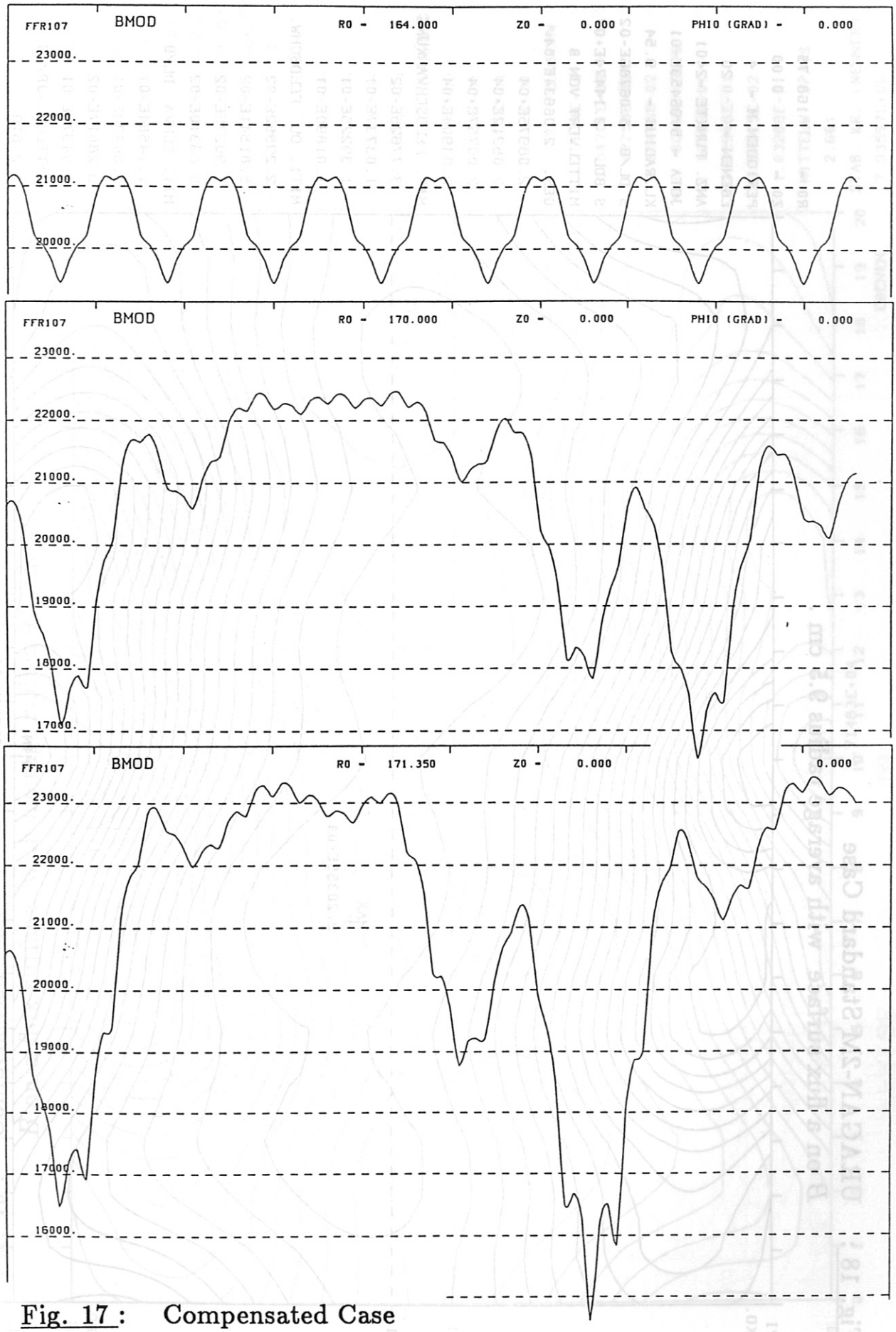

Fig. 17 : Compensated Case
B along 3 flux surfaces; 2 toroidal transits .

Fig. 18 : URAGAN-2M Standard Case
B on a flux surface with average radius 9.5 cm .

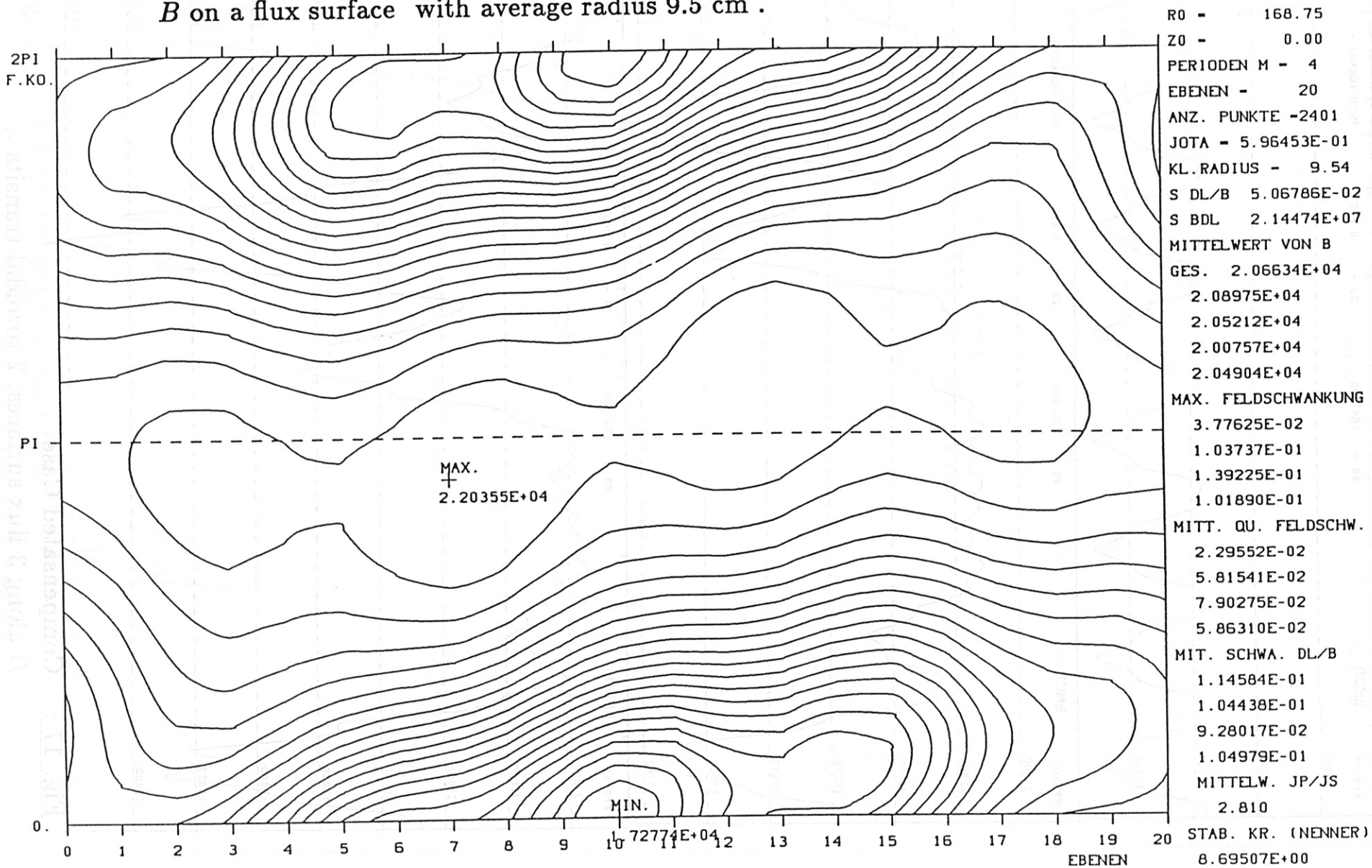

FILE2.U2M KHARKOV ST.C. HXU2M-267 15 27 39.2618 SP400/--38.5 SPOU2C333K

Fig. 19 : Compensated Case
B on a flux surface with average radius 9.7 cm .

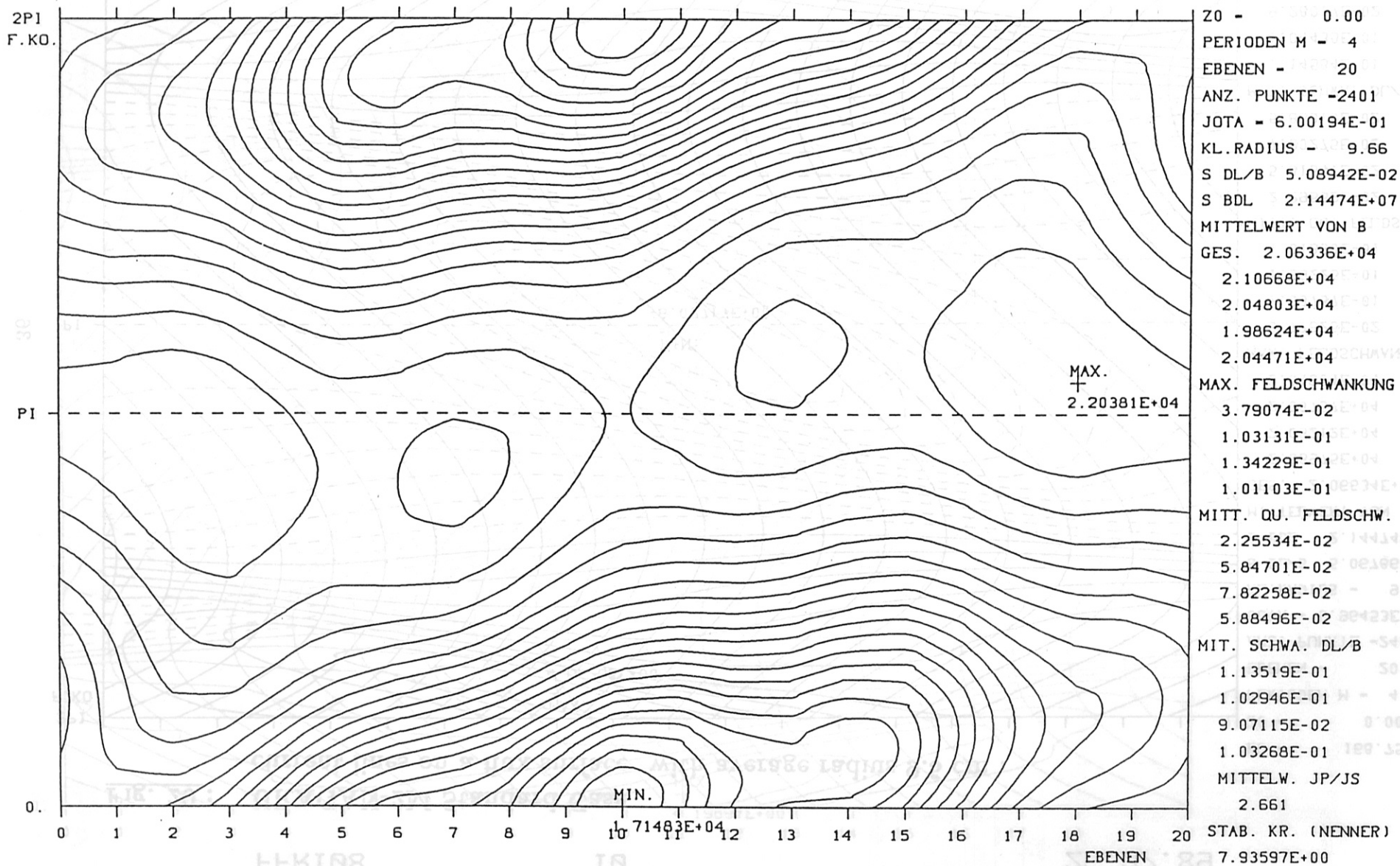

FILE2.U2M KHARKOV 0.0070 HXU2T-267 15 27 39.2618 SP400/--38.5 SPOU2C333K

Fig. 20 : URAGAN-2M Standard Case
current lines on a flux surface with average radius 9.5 cm .

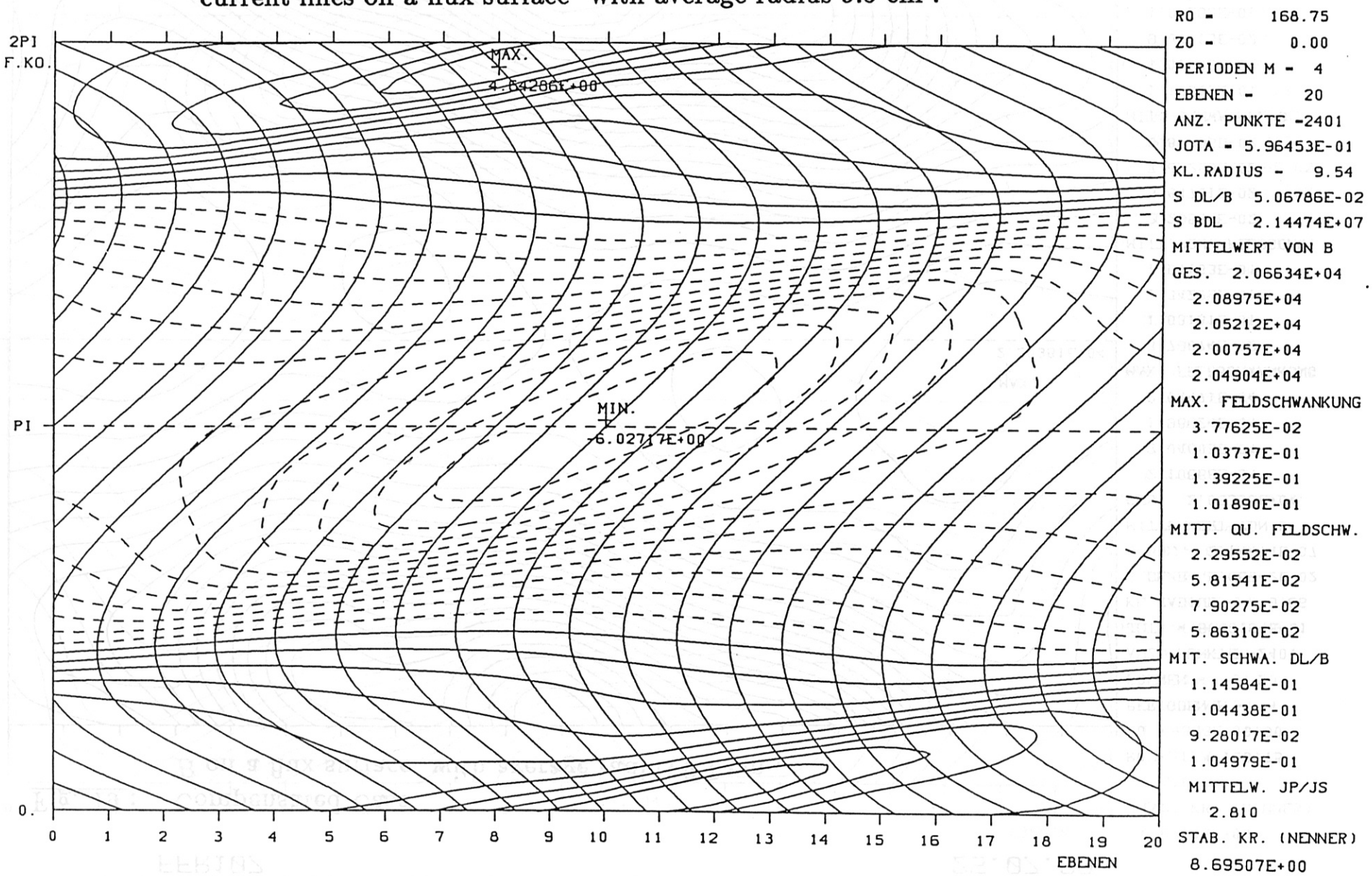

Fig. 21 : Compensated Case
current lines on a flux surface with average radius 9.7 cm .

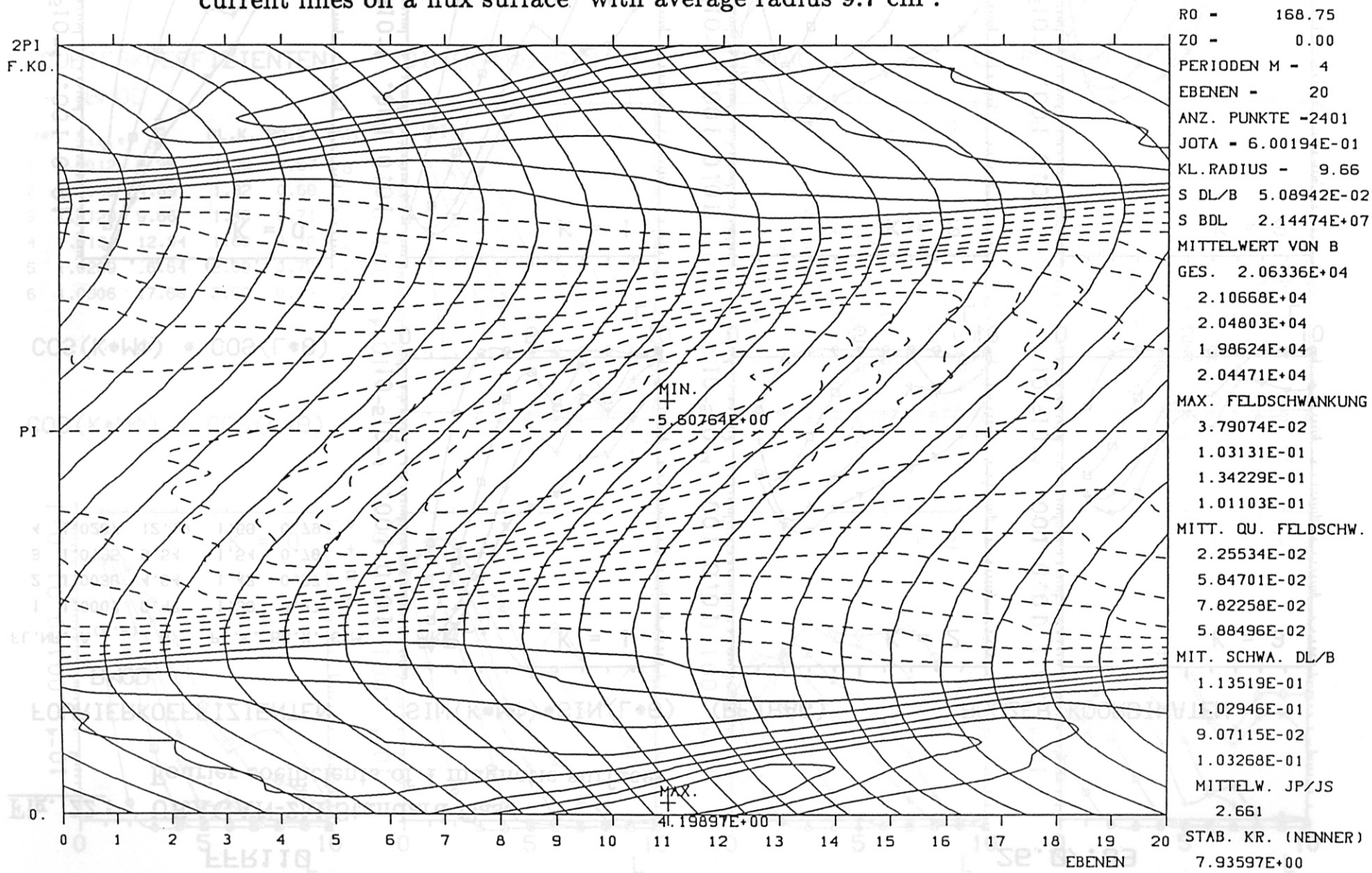

FILE2.U2M KHARKOV 0.0070 HXU2T-267 15 27 39.2618 SP400/--38.5 SPOU2C333K

Fig. 22 : URAGAN-2M Standard Case
Fourier coefficients of 4 magnetic surfaces

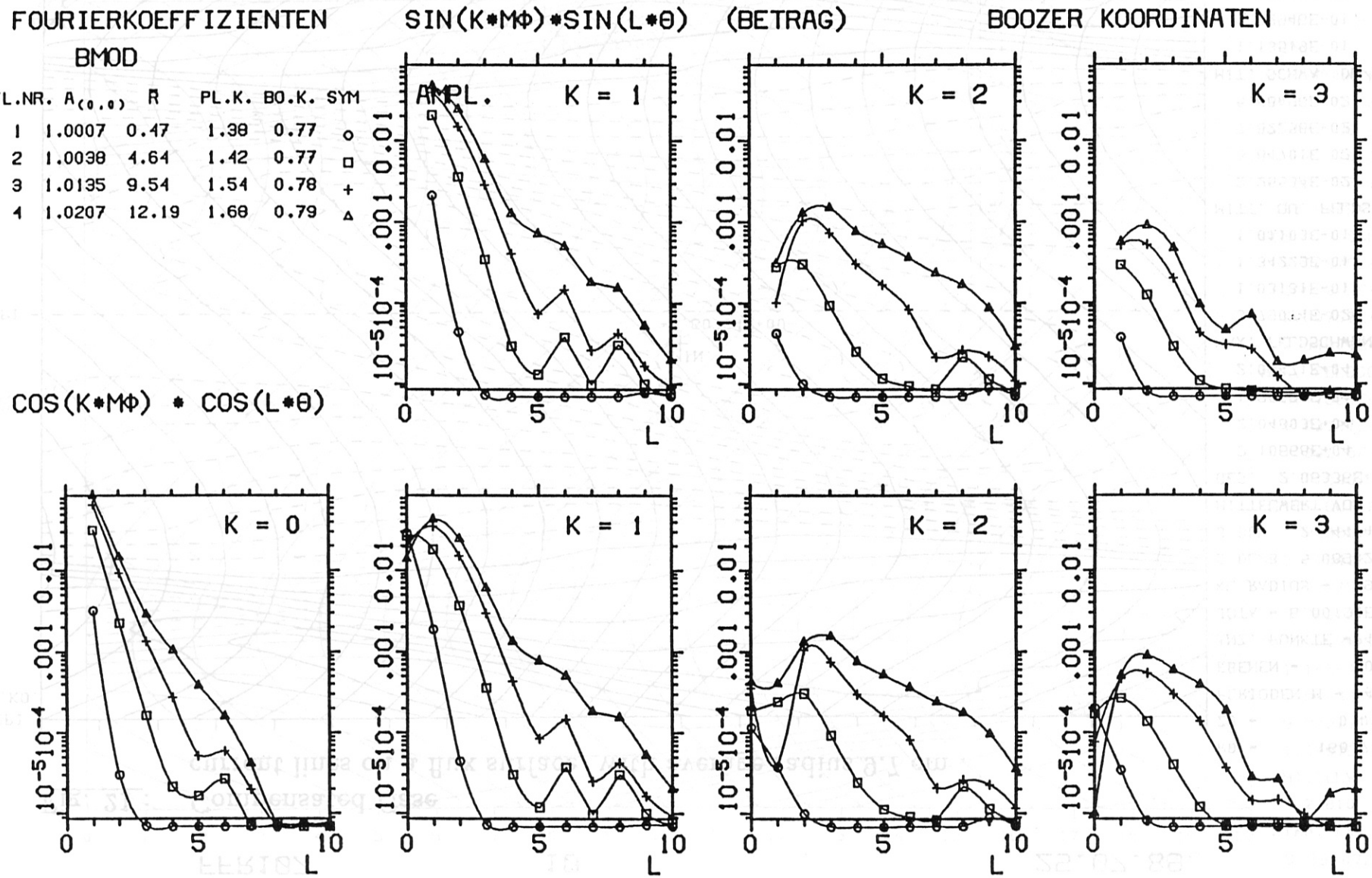

Fig. 23 : Compensated Case
Fourier coefficients of 6 magnetic surfaces

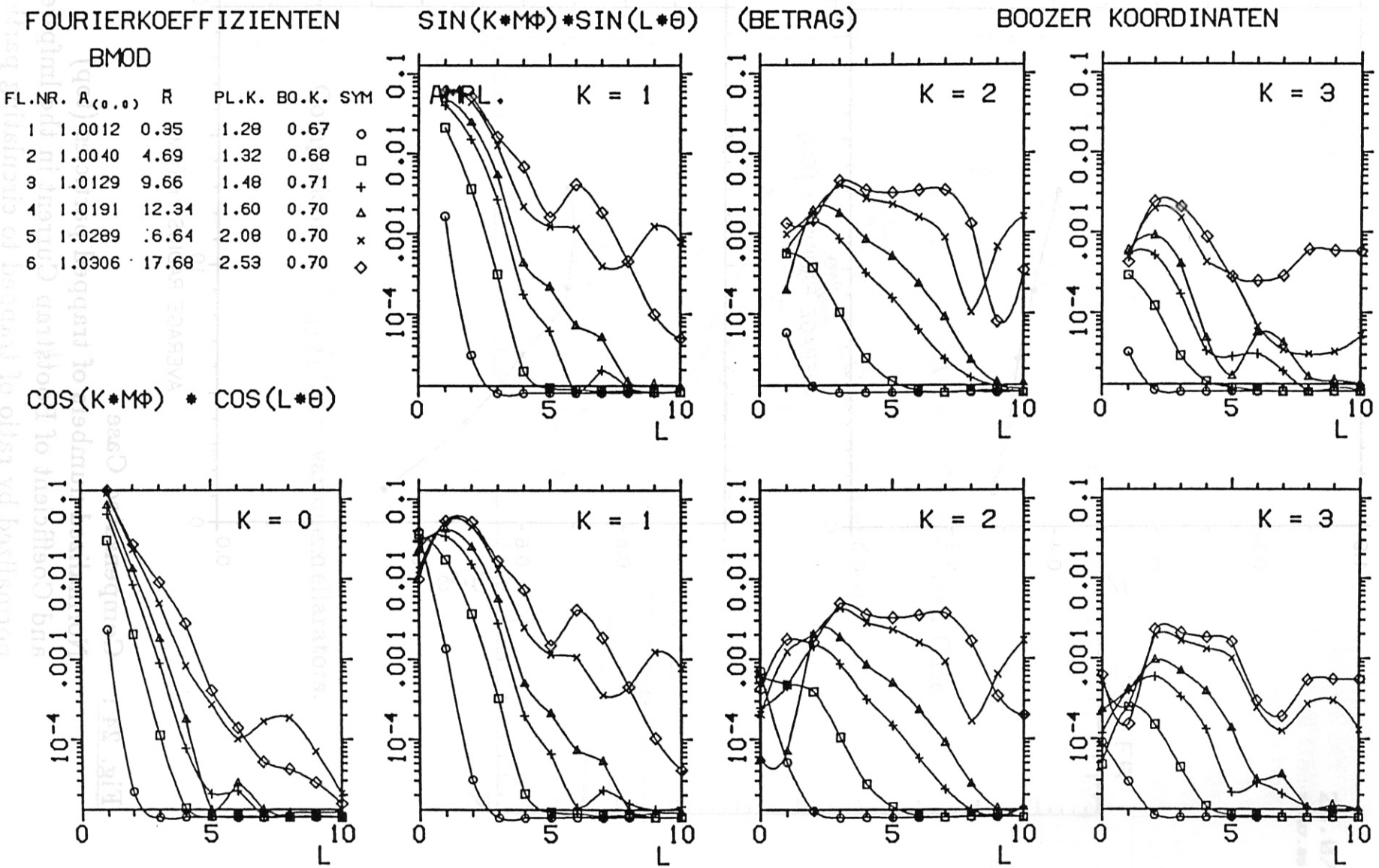

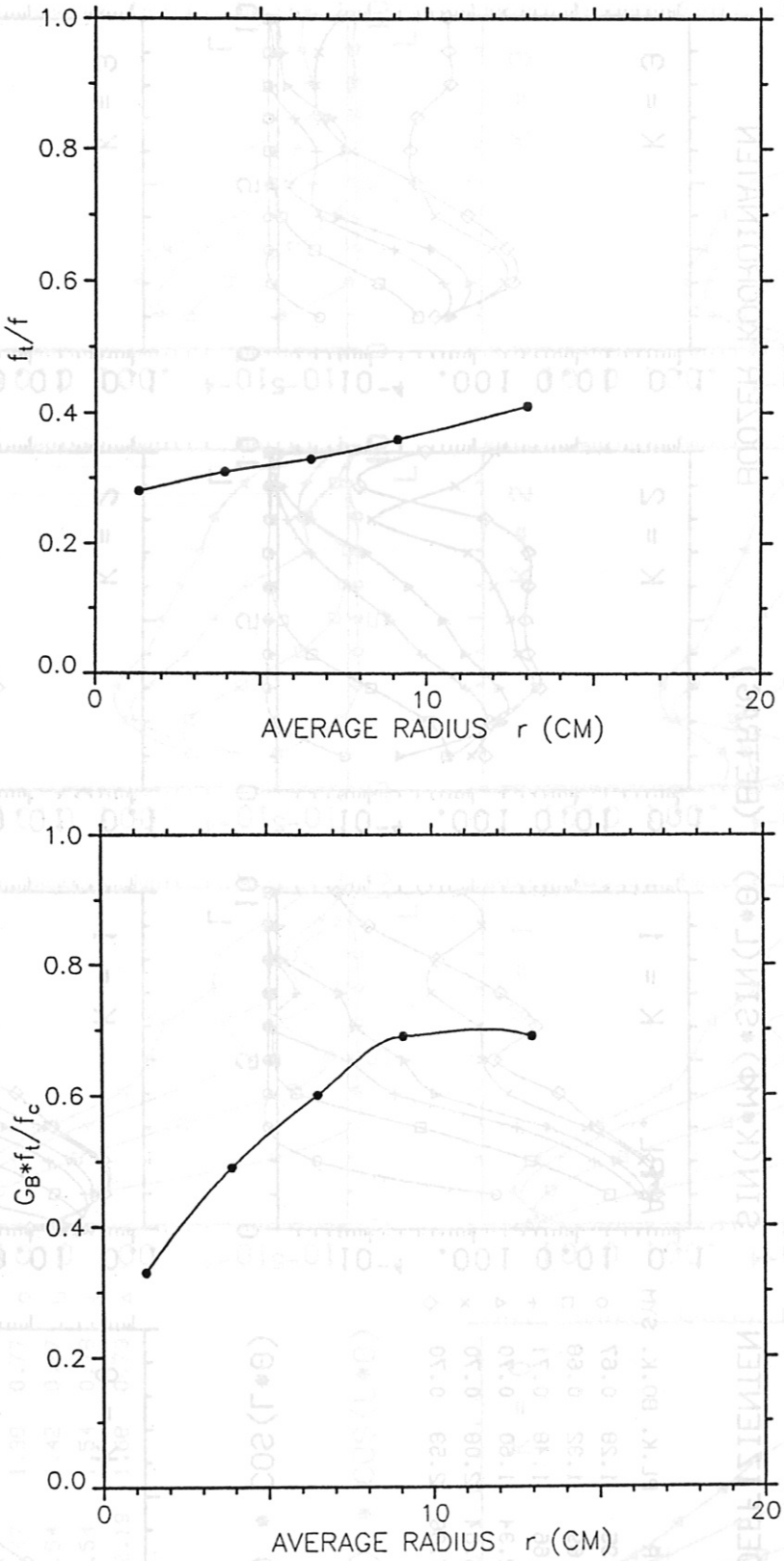

Fig. 24 : Compensated Case
Normalized numbers of trapped particles (top)
and Coefficient of Bootstrap Current in the lmfp-regime
normalized by ratio of trapped to circulating particles (bottom) .

25.07.89

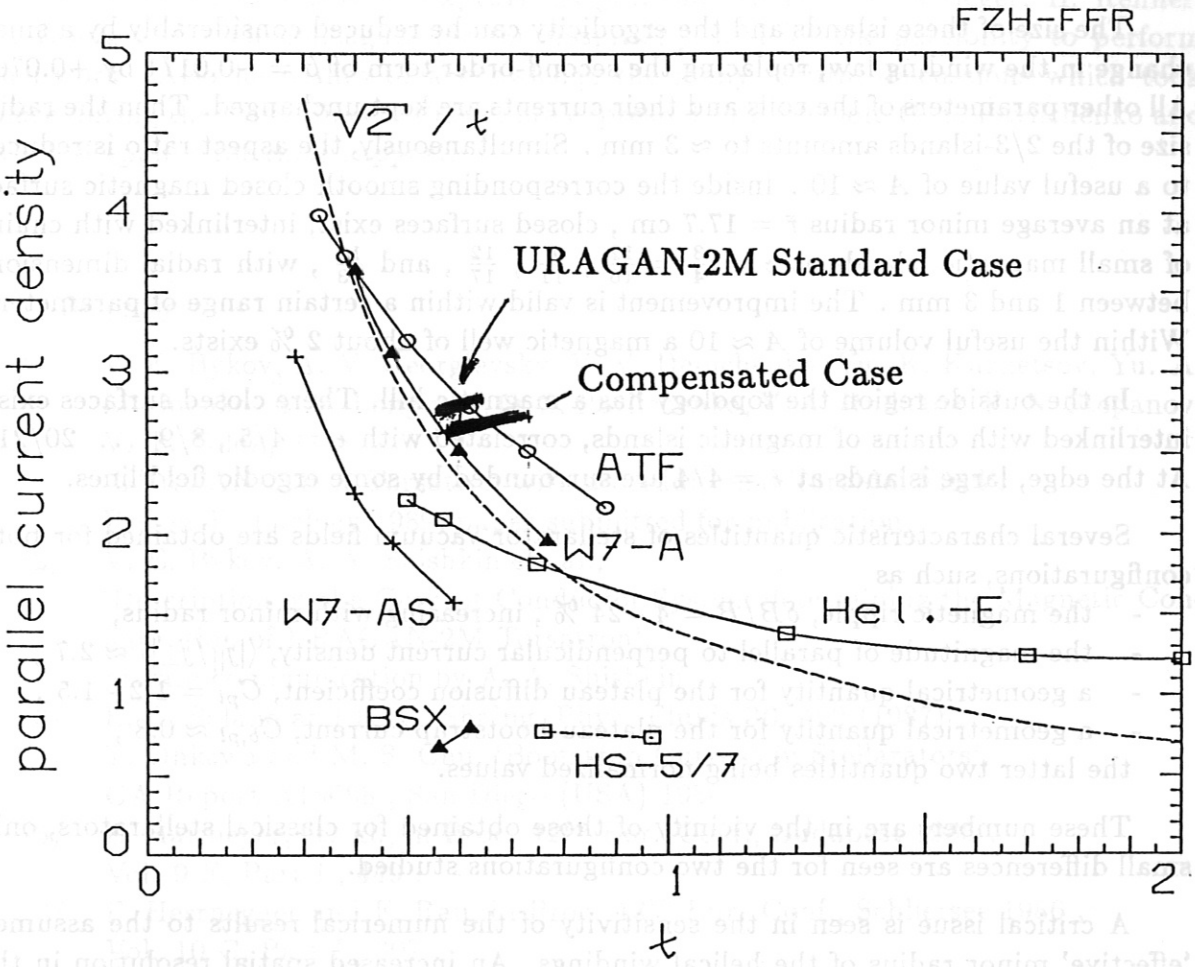

Fig. 25 : Comparison of $\langle |j_{||}/j_{\perp}| \rangle$ for various stellarators.

6.) SUMMARY AND CONCLUSIONS

The Standard Case of the torsatron experiment URAGAN-2M with an additional toroidal field coil system has been examined. The ι-profile obtained in the present report agrees reasonably with that of ref. /2/ in the inner part of the configuration, up to a minor radius of about 13.5 cm . A major issue is seen in the size of the 'natural' magnetic islands at $\iota = 2/3$, which have a radial extent of several cm . These islands occur near the edge of the configuration and are surrounded by higher-order islands and ergodic surfaces.

The size of these islands and the ergodicity can be reduced considerably by a small change in the winding law, replacing the second-order term of $\beta = -0.0171$ by $+0.070$. All other parameters of the coils and their currents are kept unchanged. Then the radial size of the 2/3-islands amounts to $\approx$ 3 mm . Simultaneously, the aspect ratio is reduced to a useful value of $A \approx 10$. Inside the corresponding smooth closed magnetic surface at an average minor radius $\bar{r} = 17.7$ cm , closed surfaces exist, interlinked with chains of small magnetic islands at $\iota = \frac{3}{4} = \frac{12}{16}$, $\frac{8}{11}$, $\frac{12}{17}$, and $\frac{16}{23}$, with radial dimensions between 1 and 3 mm . The improvement is valid within a certain range of parameters. Within the useful volume of $A \approx 10$ a magnetic well of about 2 % exists.

In the outside region the topology has a magnetic hill. There closed surfaces exist, interlinked with chains of magnetic islands, correlated with $\iota = 4/5$, $8/9$ ... $20/21$. At the edge, large islands at $\iota = 4/4$ are surrounded by some ergodic field lines.

Several characteristic quantities of stellarator vacuum fields are obtained for both configurations, such as

- the magnetic ripple, $\delta B/B = 4$ - 24 % , increasing with minor radius,
- the magnitude of parallel to perpendicular current density, $\langle |j_{||}/j_{\perp}| \rangle \approx 2.7$,
- a geometrical quantity for the plateau diffusion coefficient, $C_{pl} = 1.2$ - 1.5 ,
- a geometrical quantity for the plateau bootstrap current, $C_{b,pl} \approx 0.8$,

the latter two quantities being normalized values.

These numbers are in the vicinity of those obtained for classical stellarators, only small differences are seen for the two configurations studied.

A critical issue is seen in the sensitivity of the numerical results to the assumed 'effective' minor radius of the helical windings. An increased spatial resolution in the filamentary model of the helical windings is recommended. Several radial layers should be used, three filaments per layer are regarded as minimum. Furthermore, studies concerning the influence of symmetry breaking perturbations are of importance in order to attain a magnetic field of good quality for the URAGAN-2M device.

Acknowledgement

This report was initiated during the scientific visit of A. A. Shishkin at IPP Garching in July 1989, under the terms of the agreement on scientific and technical cooperation, dated 22 July 1986 :

'Abkommen zwischen der Regierung der Bundesrepublik Deutschland
und der Regierung der Union der Sozialistischen Sowjetrepubliken
über wissenschaftlich-technische Zusammenarbeit' .

A. A. Shishkin wishes to express his gratitude to Drs. G. Grieger, H. Renner, H. Wobig and their colleagues for the hospitality, and for the possibility to perform this work. Also he wishes to acknowledge the many fruitful discussions which took place during the visit. Sincere thanks are expressed to Professors O. S. Pavlichenko and K. N. Stepanov for their support.

References

/1/ V. E. Bykov, A. V. Georgievsky, V. V. Demchenko, Yu. K. Kuznetsov, Yu. A. Litvinenko, A. V. Longinov, O. S. Pavlichenko, V. A. Rudakov, K. N. Stepanov, V. T. Tolok,
'URAGAN-2M: A Torsatron with an Additional Toroidal Field',
Fusion Technology 1989, paper submitted for publication.

/2/ V. E. Bykov, A. A. Shishkin et. al.,
'Description of the Current Conductor System determining the Magnetic Configuration of URAGAN-2M Torsatron',
private communication by A. A. Shishkin .

/3/ E. R. Solano and K. C. Shaing, Phys. Fluids **30**, 462 (1987) .

/4/ T. Ohkawa and M. S. Chu, 'Bootstrap Current in Stellarators',
GA-Report A18688 , San Diego (USA) 1986

/5/ E. Harmeyer, et. al., in Proc. 12^{th} Eur. Conf., Budapest 1985 ,
Vol. 9 F, Part I , 449 .

/6/ F. Herrnegger and F. Rau, in Proc. 13^{th} Eur. Conf., Schliersee 1986 ,
Vol. 10 C, Part I , 307 .

/7/ E. Harmeyer, et. al., in Proc. 14^{th} Eur. Conf., Madrid 1987 ,
Vol. 11 D, Part I , 411 .

/8/ E. Harmeyer, et. al., in Proc. 15^{th} Eur. Conf., Dubrovnik 1988 ,
Vol. 12 B, Part II , 494 .

/9/ C. Beidler, et. al., in Proc. 16^{th} Eur. Conf., Venezia 1989 ,
Vol. 13 B, Part II , 595 .

/10/ C. Beidler, et. al., in Proc. 16^{th} Eur. Conf., Venezia 1989 ,
Vol. 13 B, Part II , 679 .

/11/ F. Herrnegger, private communication .